Eales, S, Fullard, A, Allen, M, Smith, MWL, Baldry, IK, Bourne, N, Clark, CJR, Driver, S, Dunne, L, Dye, S, Graham, AW, Ibar, E, Hopkins, A, Ivison, R, Kelvin, LS, Maddox, S, Maraston, C, Robotham, ASG, Smith, D, Taylor, EN, Valiante, E, Werf, PVD, Baes, M, Brough, S, Clements, D, Cooray, A, Gomez, H, Loveday, J, Phillipps, S, Scott, D and Serjeant, S

 H-ATLAS/GAMA: Quantifying the Morphological Evolution of the Galaxy Population Using Cosmic Calorimetry

https://researchonline.ljmu.ac.uk/id/eprint/1719/

Article

H-ATLAS/GAMA: Quantifying the Morphological Evolution of the Galaxy Population Using Cosmic Calorimetry

Stephen Eales[1][*], Andrew Fullard[1], Matthew Allen[1], M.W.L. Smith[1],
Ivan Baldry[2], Nathan Bourne[3], C.J.R. Clark[1], Simon Driver[4], Loretta Dunne[3,5],
Simon Dye[6], Alister W. Graham[7], Edo Ibar[8], Andrew Hopkins[9],
Rob Ivison[3,10], Lee S. Kelvin[11], Steve Maddox[3,5], Claudia Maraston[12],
Aaron S.G. Robotham[13], Dan Smith[14], Edward N. Taylor[15], Elisabetta Valiante[1],
Paul van der Werf[16], Maarten Baes[17], Sarah Brough[9], David Clements[18],
Asantha Cooray[19], Haley Gomez[1], Jon Loveday[20], Steven Phillipps[21], Douglas Scott[22]
and Steve Serjeant[23]

[1] *School of Physics and Astronomy, Cardiff University, The Parade, Cardiff CF24 3AA, UK*
[2] *Astrophysics Research Institute, Liverpool John Moores University, IC2,*
Liverpool Science Park, 146 Brownlow Hill, Liverpool L3 3RF, UK
[3] *Institute for Astronomy, The University of Edinburgh, Royal Observatory, Blackford Hill, Edinburgh, EH9 3HJ, UK*
[4] *International Centre for Radio Astronomy Research, 7 Fairway, The University of Western*
Australia, Crawley, Perth, WA 6009, Australia
[5] *Department of Physics and Astronomy, University of Canterbury, Christchurch, New Zealand*
[6] *School of Physics and Astronomy, University of Nottingham, University Park, Nottingham NG7 2RD, UK*
[7] *Centre for Astrophysics and Supercomputing, Swinburne University of Technology, Hawthorn, Victoria 3122, Australia*
[8] *Instituto de Física y Astronomía, Universidad de Valparaíso, Avda. Gran Bretaña 1111, Valparaíso, Chile*
[9] *Australian Astronomical Observatory, PO Box 915, North Ryde, NSW 1670, Australia*
[10] *European Southern Observatory, Karl-Schwarzschild-Strasse 2, 85748, Garching, Germany*
[11] *Institut fur Astro- und Teilchenphysik, Universitat Innsbruck, Technikerstrasse 25, A-6020 Innsbruck, Austria*
[12] *Institute of Cosmology and Gravitation (ICG), University of Portsmouth, Dennis Sciama Building, Burnaby Road,*
Portsmouth PO1 3FX, UK
[13] *Scottish Universities Physics Alliance, School of Physics and Astronomy, University of St. Andrews, North Haugh,*
St. Andrews KY16 9SS, UK
[14] *Centre for Astrophysics Research, Science and Technology Research Institute, University of Hertfordshire, Hatfield,*
Herts, AL10 9AB, UK
[15] *School of Physics, The University of Melbourne, Parkville, VIC 3010, Australia*
[16] *Leiden Observatory, PO Box 9513, 2300 RA Leiden, the Netherlands*
[17] *Sterrenkundig Observatorium,Universiteit Gent, Krijgslaan 281 S9, B-9000 Gent, Belgium*
[18] *Astrophysics Group, Imperial College, Blackett Laboratory, Prince Consort Road, London SW7 2AZ*
[19] *Department of Physics and Astronomy, University of California, Irvine, CA 92697, USA*
[20] *Department of Physics and Astronomy, University of Sussex, Falmer Campus, Brighton BN1 9QH UK*
[21] *Astrophysics Group, Department of Physics, University of Bristol, Tyndall Avenue, Bristol BS8 1TL*
[22] *Department of Physics and Astronomy, University of British Columbia, 6224 Agricultural Road, Vancouver,*
BC V6T 1Z1, Canada
[23] *Department of Physical Science, The Open University, Milton Keynes, MK7 6AA, UK*

arXiv:1506.05466v2 [astro-ph.GA] 19 Jun 2015

ABSTRACT

Using results from the Herschel Astrophysical Terrahertz Large-Area Survey and the Galaxy and Mass Assembly project, we show that, for galaxy masses above $\simeq 10^8\ M_\odot$, 51% of the stellar mass-density in the local Universe is in early-type galaxies (ETGs: Sérsic $n > 2.5$) while 89% of the rate of production of stellar mass-density is occurring in late-type galaxies (LTGs: Sérsic $n < 2.5$). From this zero-redshift benchmark, we have used a calorimetric technique to quantify the importance of the morphological transformation of galaxies over the history of the Universe. The extragalactic background radiation contains all the energy generated by nuclear fusion in stars since the Big Bang. By resolving this background radiation into individual galaxies using the deepest far-infrared survey with the Herschel Space Observatory and a deep near-infrared/optical survey with the Hubble Space Telescope (HST), and using measurements of the Sérsic index of these galaxies derived from the HST images, we estimate that $\simeq$83% of the stellar mass-density formed over the history of the Universe occurred in LTGs. The difference between this and the fraction of the stellar mass-density that is in LTGs today implies there must have been a major transformation of LTGs into ETGs after the formation of most of the stars.

Key words: galaxies: bulges, evolution, star formation

1 INTRODUCTION

Over the last decade much of the research on galaxy evolution has started from the paradigm that there are two types of galaxy: star-forming galaxies and passive or quiescent galaxies in which stars are no longer forming. In this paradigm star-forming galaxies lie on the Galaxy Main Sequence (GMS) until some catastrophic process (or at least, a process brief compared to the age of the Universe) quenches the star formation, causing the galaxy to move away from the GMS and become a 'red and dead' galaxy (e.g. Peng et al. 2010; Speagle et al. 2014).

The rapid evolution of the stellar mass function of passive galaxies since $z \sim 1-2$, relative to the much slower evolution of the stellar mass function of star-forming galaxies (Faber et al. 2007; Muzzin et al. 2013; Ilbert et al. 2013), implies that the formation of passive galaxies occurred after the epoch at which the star-formation rate in the Universe was at its peak (Hopkins and Beacom 2006). This temporal sequence is circumstantial evidence that passive galaxies were formed from the star-forming population. A more quantitative argument is that Peng et al. (2010) have shown that the shapes of the two stellar mass functions are exactly what one would predict from a simple model in which passive galaxies are formed by the quenching of the star formation in the galaxies in the star-forming population.

In an accompanying paper (Eales et al. 2015), we show that when this paradigm is considered in the light of the galaxies detected by the Herschel Space Observatory (Pilbratt et al. 2010) it looks less convincing. Approximately 25% of the galaxies detected at low redshift by the largest Herschel extragalactic survey, the Herschel ATLAS (Eales et al. 2010), are galaxies that would have been classified as quiescent or passive using optical criteria, but still have large reservoirs of interstellar material and are still forming stars. They are red but not dead. The blurring of this dichotomy when viewed from a far-infrared perspective is, we argue,

evidence that some more gradual physical processes (rather than catastrophic quenching) are necessary to explain the properties of the galaxy population (Eales et al. 2015). At the very least, our results show that there is a major practical problem in measuring star-formation rates in galaxies and in separating galaxies into the two classes, which may explain the huge diversity in measurements of the shape and evolution of the GMS found by Speagle et al. (2014) in their meta-analysis of 25 separate studies of the GMS.

In this paper we consider a different dichotomy: that between early-type and late-type galaxies (henceforth ETGs and LTGs). The terms 'early type' and 'late type' were coined by Hubble (Hubble 1926, 1927), although he did not mean the terminology to indicate that ETGs evolve into LTGs (Baldry 2008). ETGs are galaxies with a prominent spheroid or bulge, in particular classes E and S0 in the Hubble morphological classification, whereas the structures of LTGs are dominated by a spiral pattern. We discuss below how to turn this rather vague definition into one that is more quantitative. Although there is an obvious dichotomy between elliptical galaxies and late-type spirals when looking at optical images, the dichotomy between ETGs and LTGs is much less obvious when galaxies are studied more closely. Integral-field kinematic studies have shown that ETGs can be split into slow and fast rotators, with the kinematic properties of the fast rotators being similar to those of LTGs and the slow rotators being much rarer than the fast rotators (Emsellem et al. 2011). Careful quantitative analysis of the images of ETGs also often reveals that the galaxy has a disk even when this is not apparent from simply looking at the image (Krajnovic et al. 2013). Observations with the Herschel Space Observatory have revealed that $\simeq$50% of ETGs contain dust, and that there is gradual change of the dust properties of galaxies as one moves along the Hubble Sequence from LTGs to ETGs, rather than a sudden jump at the transition from late types to early types (Smith et al. 2012a).

Although Hubble did not draw any conclusions about the evolutionary links between ETGs and LTGs, there are

* E-mail: sae@astro.cf.ac.uk

many theoretical arguments for why galaxy evolution is expected to include the morphological transformation of galaxies. Almost four decades ago, Toomre (1977) suggested that the merger of two LTGs might scramble the stars and velocity fields, leading to the formation of an ETG supported against gravity by the random velocities of the stars rather than by the rotation of a galactic disk. On the other hand, if one starts with a spheroid, it seems likely that the accretion of gas and angular momentum from the intergalactic medium is likely to lead to the growth of a disk (Combes et al. 2014 and references therein). A recent idea is that a spheroid is formed by the rapid motion of star-forming clumps towards the centre of a disk (Noguchi 1999; Bournaud et al. 2007; Genzel et al. 2011, 2014; Dekel and Burkert 2014), transforming a LTG into an ETG, with the growth of the spheroid eventually stopping the formation of stars in the disk once the spheroid has enough mass to stabilize the disk against gravitational collapse (Martig et al. 2009).

There is substantial overlap between ETGs and the class of passive galaxies and between LTGs and the class of star-forming galaxies. The overlap between the classes in the low-redshift Universe is well known (Kennicutt 1998), but over the last decade a large number of observational programmes with the Hubble Space Telescope (HST) have shown that this is also true at high redshift: high-redshift passive galaxies tend to have spheroidal structures and the structures of high-redshift star-forming galaxies are generally dominated by disks (Bell et al. 2004a; Wuyts et al. 2011; Bell et al. 2012; Bruce et al. 2012; Buitrago et al. 2013; Szomoru et al. 2013; Tasca et al. 2014). These studies show that the evolutionary process that produces passive galaxies must be linked to the evolutionary process that generates spheroids (Bell et al. 2012).

These HST studies have two limitations. The first limitation is a consequence of the extragalactic background radiation and of the nature of the sources which constittue it. The extragalactic background radiation (Dole et al. 2006; Dwek and Krennrich 2013) is dominated by radiation of roughly equal strength in two wavebands, in the optical/near-infrared and in the far-infrared at $\simeq 100 - 200$ μm. This equality implies that $\simeq 50\%$ of the energy emitted by stars since the Big Bang has been absorbed by dust and is now in the far-infrared band. This is an average value and studies of the relative cosmic evolution of the far-infrated and UV luminoisity density (Takeuchi, Buat and Burgarella 2005; Burgarella et al. 2013) imply that the fraction of the stellar light absorbed by dust is much higher at $z > 1$ during the epoch in which most of the stars in the Universe were formed. An important difference between the two peaks is that the sources that constitute the far-infrared background are rarer and consequently more luminous. We show in this paper that in a small area of sky the optical/near-infrared background is composed of $\simeq 8000$ sources but the far-infrared background, which is of roughly equal strength, is composed of only $\simeq 1500$ sources, implying that the sources of the far-infrared background are a factor of $\simeq 5$ more luminous than the more common sources composing the optical/near-infrared background.

All of the HST studies above start from optical/near-infrared samples of galaxies. They all attempt to allow for the star-formation in each galaxy that is hidden by dust by using either the optical/near-infrared colours of the galaxy

to estimate the extinction or, in two cases, the Spitzer 24-μm observations to estimate the far-infrared emission. The probem with the first method is that the luminous galaxies that make up the far-infrared background are so shrouded by dust that estimates of their star-formation rates from short-wavelength measurements are likely to be inaccurate. The problem with the second is the significant extrapolation necessary from the mid-infrared to the far-infrared.

The second limitation of these studies is that all only reach conclusions about the morphologies of the galaxies in restricted samples, with the usual limits being redshift and stellar mass. As one example, Bruce et al. (2012) concluded that the star-forming galaxies in the redshift range $2 < z < 3$ and with stellar masses $> 10^{11}$ $M_\odot$ have structures that are dominated by disks. Although conclusions like this are important, they always leave open the possibility that most of the stars in the Universe were formed in a different range of redshift or in galaxies with stellar masses outside the limits of the sample. Our overall goal in this paper is to reach a more general conclusion about the fraction of the stellar mass-density that was formed in galaxies of different morphological types over the entire history of the Universe.

To reach this conclusion, we have used a calorimetry technique, which is not new (Pagel et al. 1997; Lilly and Cowie 1987) but is particularly timely because of one of the successes of the Herschel Space Observatory. The method is based on the fact that the extragalactic background radiation is the repository of all the radiation emitted as the result of nuclear fusion in stars. For the method to be practical, it is necessary to resolve this background radiation into individual sources. Deep surveys with the Hubble Space Telescope had already resolved the optical/near-infrared background into individual sources, and now the deepest Herschel survey has also achieved this goal in the far infrared (Elbaz et al. 2011; Magnelli et al. 2013; Leiton et al. 2015).

One of the advantages of the calorimetry technique is that it does not require us to estimate the star-formation rate in individual galaxies, which is difficult enough even for galaxies at zero redshift (Kennicutt 1998; Kennicutt and Evans 2012). For example, one method of estimating the star-formation rate in a galaxy is by assuming the far-infrared emission represents the bolometric luminosity of newly formed stars (Kennicutt 1998; Kennicutt and Evans 2012). This is probably a reasonable assumption for the luminous galaxies that constitute the far-infrared background but it is clearly wrong in galaxies with low star-formation rates, in which much of the far-infrared emission is from dust heated by the old stellar population (Bendo et al. 2015). The calorimetry method avoids the need to make assumptions like this by linking the total energy emitted by a galaxy to the energy produced by nuclear fusion.

Our secondary goal in this paper is to determine how the stellar mass-density in the Universe today depends on galaxy morphology. By comparing this distribution with the result from the caloriometry technique on the morphologies of the galaxies in which most stars were formed, it is possible to quantify how important the transformation of galaxy morphology has been in the evolution of the galaxy population.

We have achieved this secondary goal using two new wide-field surveys of the nearby Universe. The Herschel Astrophysical Terrahertz Large Area Survey (the Herschel-

ATLAS or H-ATLAS, Eales et al. 2010) is the Herschel extragalactic survey covering the largest area of sky, 550 square degrees, roughly one eightieth of the entire sky. The survey consists of images at 100, 160, 250, 350 and 500 μm of five fields, two large fields at the North and South Celestial Poles (NGP and SGP) and three smaller fields on the celestial equator. The NGP and the equatorial fields were covered in the Sloan Digital Sky Survey, but more importantly the equatorial fields have also been covered by a much deeper spectroscopic survey, the Galaxy and Mass Assembly (GAMA) redshift survey (Driver et al. 2011). The GAMA team has produced many different data products for the galaxies in their survey, and we have made liberal use of these data products in our investigation.

One of the challenges in an investigation like this is to find a quantitative measure of galaxy morphology that can be used over a large range of redshift. The obvious way to measure the position of a galaxy on the morphological spectrum from early-type to late-type is to measure the relative proportions of the stellar mass that is in the bulge/spheroid and the disk. However, there are two major practical problems with doing this. The first is that although for many years it was believed that the spheroids of galaxies are described by the de Vauclouleur $R^{1/4}$ model (de Vaucouleurs 1948), it is now realised that galaxy bulges follow a range of intensity profiles (Graham 2013 and references therein). Second, estimates of the proportion of the galaxy's stellar mass that is in the bulge depend strongly on the assumptions made about the dust extinction within the galaxy (Driver et al. 2008; Graham and Worley 2008), which requires great care and spatial resolution to measure accurately.

We have instead used the simpler approach of using the Sérsic index as a measure of a galaxy's morphology. The Sérsic function is

$$I(r) = I_e exp(-b_n[(\frac{r}{r_e})^{1/n} - 1]) \qquad (1)$$

in which I_e is the intensity at the effective radius, r_e, that contains half of the total light from the model, n is the Sérsic index and b_n is a function that depends on n (Sérsic 1963; Graham and Driver 2005). This useful function can be used to fit the structures of all galaxy types. If the value of the Sérsic index is one, the Sérsic profile becomes an exponential intensity profile, which in the low-redshift Universe is the intensity profile followed by a disk. If the value of the Sérsic index is four, the Sérsic profile becomes the de Vauclouleur $R^{1/4}$ profile, which is the intensity profile followed by ellipticals in the low-redshift Universe. The advantage of adopting this method of measuring the structure of a galaxy compared to measuring the bulge-to-disk ratio is that it is much simpler, not requiring any assumptions about the effect of dust extinction or the bulge profile (Graham and Worley 2008).

In Section 2, we describe our investigation of how the stellar mass-density and star-formation rate per unit comoving volume depend on galaxy morphology in the Universe today. Section 3 describes the caloriometry method that we have used to estimate how the mass of stars that has formed over the history of the Universe depends on the morphology of the galaxy in which those stars were formed. Section 4 gives the results of the calorimetry method. The results and

their implications are discussed in §5 and the conclusions are given in §6. We assume the cosmological parameters given from the Planck 2013 cosmological analysis (Planck Collaboration XVI 2014): a spatially-flat universe with $\Omega_M = 0.315$ and a Hubble constant of 67.3 km s^{-1} Mpc^{-1}.

2   THE UNIVERSE TODAY

2.1   The relationship between star-formation density and morphology

In order to carry out a census of star formation, it seems sensible to start from a far-infrared survey, since newly formed stars are hidden by dust from optical telescopes. This procedure might lead to the star-formation rate being underestimated if there is a population of galaxies in which stars are forming but in which there is little dust. However, we show in an accompanying paper that at low redshifts we do not appear to be missing any star-forming but dust-free galaxies (Eales et al. 2015).

We have therefore used as our starting point the far-infrared H-ATLAS survey rather than the optical GAMA survey. We have used the data for the H-ATLAS equatorial fields (Eales et al. 2010), which are also covered by the GAMA survey and have a total area of $\simeq$160 deg^2. The version of the H-ATLAS data used in this paper is the Phase 1 version 3 internal data release, which was obtained using very similar methods to those used for the H-ATLAS Science Demonstration Phase, rather than the public data release described by Valiante et al. (2015) and Bourne et al. (2015). The maps at 250, 350 and 500 μm were made using the methods described by Pascale et al. (2011) and the maps at 100 and 160 μm were made using the method described in Ibar et al. (2010). The detection of the sources was performed on the 250-μm images using the methods described in Rigby et al. (2011). Flux measurements at 350 and 500 μm were generally made by measuring the fluxes at the 250-μm positions on the 350-μm and 500-μm images after convolving the latter images with the point spread function of the telescope. We measured fluxes on the less sensitive 100 and 160-μm images using aperture photometry, with an aperture diameter chosen to maximise the signal-to-noise for point sources. For the small percentage of H-ATLAS sources associated with nearby galaxies, we measured flux densities by carrying out aperture photometry at all wavelengths with an aperture diameter chosen to recover, as nearly as possible, all the flux.

The Phase 1 catalogue consists of the 109,231 sources detected at $> 5\sigma$ at either 250, 350 or 500 μm (the maps at 100 and 160 μm are much less sensitive than those at longer wavelengths). These signal-to-noise limits corresponds to flux densities at 250, 350 and 500 μm of 32, 36 and 45 mJy, respectively.

As in the Science Demonstration Phase, we used a likelihood-ratio analysis (Smith et al. 2011) to match the sources to galaxies in the Sloan Digital Sky Survey (SDSS, DR7; Abazajian et al. 2009) with $r < 22.4$. With this method, we can estimate the probability (the reliability - R) of a galaxy being the true association of a submillimetre source. We treat galaxies with $R > 0.8$ as being likely counterparts to the submillimetre sources. There are counterparts with $R > 0.8$ for 29,761 of the 104,657 sources detected

at 5σ at 250 μm. Of these counterparts 14,917 have spectroscopic redshifts, mostly from the GAMA redshift survey but some from the SDSS. For the counterparts, there is matched-aperture photometry in u, g, r, i and z from the SDSS; in Y, J, H and K from the UKIRT Large Area Survey, which is part of the UKIRT Infrared Deep Sky Survey (Lawrence et al. 2007); and in near-ultraviolet and far-ultraviolet filters from the Galaxy Evolution Explorer (Martin et al. 2005). We have used the photometry to estimate photometric redshifts using the artificial neural network code ANNZ (Smith et al. 2011).

Our base sample for the analysis in this paper is the 2250 Herschel sources detected at $> 5\sigma$ at 250 μm in the fields common to H-ATLAS and GAMA that have reliable optical counterparts with spectroscopic redshifts < 0.1. The fraction of Herschel sources for which we can find counterparts using the likelihood technique declines with the redshift of the source, but at $z < 0.1$ the fraction of sources with identified counterparts should be close to 100% (Smith et al. 2011). Virtually all the counterparts below this redshift have spectroscopic redshifts (Smith et al. 2011).

We have estimated the key properties of each galaxy, in particular its star-formation rate, from the galaxy's spectral energy distribution—the 11 photometric measurements listed above plus the five measurements in the Herschel bands—using the galaxy model MAGPHYS (Da Cunha, Charlot and Elbaz 2008). Some of the characteristics of MAGPHYS important for our analysis are that it takes account of both the star formation that is seen directly in the optical waveband and the star formation that is hidden by dust, and that the model spectral energy distribution is fit to the observed spectral energy distribution using a probabilistic method, which explores a very large number of possible star-formation histories and leads to a probability distribution for each galaxy property. Further details of the application of MAGPHYS to the H-ATLAS galaxies are given in Smith et al. (2012b). We use the median estimate of the star-formation rate for each galaxy, SFR_i, derived from the probability distribution of the star-formation rate produced by MAGPHYS.

Our estimate of the star-formation rate per unit comoving volume in the Universe today is then

$$SFR\ density = \sum_i \frac{SFR_i}{V_i} \qquad (2)$$

in which V_i is the accessible volume in which the galaxy could have been detected in the HATLAS survey. In calculating the accessible volume, we assume that the spectral energy distribution of the galaxy in the Herschel bands follows a modified black body, with the dust temperature and emissivity index both a linear function of the logarithm of the 250-μm monochromatic luminosity (Eales et al. in preparation). However, at such low redshifts our estimate of the accessible volume of a galaxy depends only very weakly on the assumption made about its spectral energy distribution.

The GAMA team has measured the value of the Sérsic index for all these galaxies from images in nine different passbands (Kelvin et al. 2012). They find that there is a small increase in the measured value of the Sérsic index when the wavelength of the image used to measure the Sérsic index
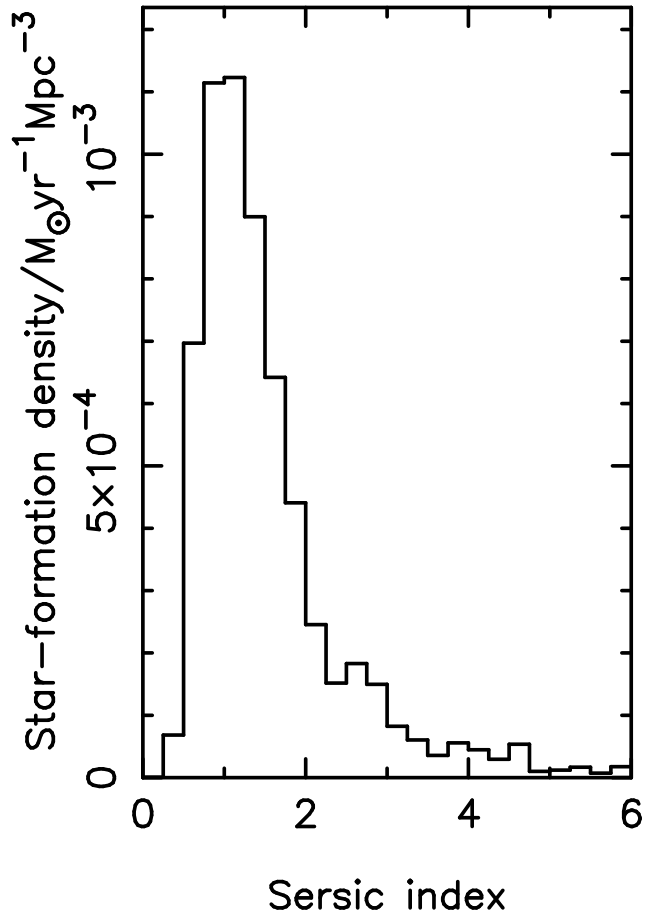
Figure 1. Star-formation rate per unit comoving volume in the Universe today as a function of Sérsic index.

is increased. We have used the values they have measured from the SDSS r-band images, since this band corresponds well to the typical rest-frame wavelength of the images used to estimate the Sérsic indices of the high-redshift galaxies (§3.5). We have measured how the star-formation rate per unit comoving volume in the Universe today depends on the Sérsic index of the galaxy in which the stars are forming by restricting the sum in equation 2 to the galaxies that fall in each bin of Sérsic index (Fig. 1). The figure shows that today the star-formation rate per unit comoving volume peaks at a Sérsic index of $\simeq 1$, implying that, today in the Universe, most stars form in galaxies that are dominated by a disk.

2.2 The relation between stellar mass-density and morphology

We can estimate the stellar mass-density as a function of Sérsic index in a similar way. This time we have started from the optical GAMA survey, since there are many ETGs that contain large stellar masses but which are forming stars at a slow rate, have little dust, and are difficult to detect with Herschel. We have started from the GAMA I database, which includes galaxies with r-band magnitudes brighter than 19.4 in the GAMA9 and GAMA15 fields and 19.8 in the GAMA15 fields. We exclude galaxies with $z < 0.002$, since their velocities are likely to have a significant component

from peculiar motions. Our sample is the 15724 galaxies with spectroscopic redshifts in the redshift range $0.002 < z < 0.1$. The stellar mass-density in the Universe today is given by

$$Stellar\ mass\ density = \sum_i \frac{M_{*i}}{V_i} \qquad (3)$$

in which M_{*i} is the stellar mass of the i'th galaxy and V_i is again accessible volume. We have used the stellar masses for the galaxies derived by Taylor et al. (2011), since there are not yet MAGPHYS estimates of the stellar mass for all the GAMA galaxies. For the H-ATLAS galaxies, for which there are estimates from both methods, there is a systematic offset of 0.17 in $log_{10}(stellar\ mass)$ between the two estimates, but once this offset is corrected for, the agreement is good, with a root-mean-squared discrepancy of 0.13 in $log_{10}(stellar\ mass)$ between the two estimates (Eales et al. 2015). The offset is not important for this analysis in this section. We have calculated the accessible volume for each galaxy using an optical spectral energy distribution derived for each galaxy from its multi-band photometry (Taylor et al. 2011). We can estimate the dependence of stellar mass density on Sérsic index by restricting the sum in equation 3 to the galaxies that fall in each bin of Sérsic index. Figure 2 shows the stellar mass-density in the Universe today as a function of Sérsic index.

As we discussed in §1, there is no agreement about the best way to separate ETGs and LTGs. In this paper, we use the operational definition that ETGs and LTGs are galaxies with a Sérsic index greater than and less than 2.5, respectively - a definition which has been used often in the literature (e.g. Shen et al. 2003; Barden et al. 2005; Buitrago et al. 2013). One argument suggests that it is a definition which has some physical meaning. Figure 1 shows that the distribution of star-formation rate per unit comoving volume is fairly symmetric, with a peak at $n = 1$. This value of n is the one expected if the structure of the galaxy is dominated by an exponential disk, suggesting that the physical meaning of the peak is that star formation mostly occurs in disk-dominated galaxies. Therefore it seems reasonable to devise an ETG/LTG classification that puts this peak in one class. With a dividing line of $n = 2.5$, the galaxies in this peak all fall in the class of LTGs, but with a lower value of n some of the galaxies in this peak would be classified as ETGs; and with a higher value of n some of the galaxies that are outside this peak would be classified as LTGs. Nevertheless, despite this argument, our definition is basically an operational one that allows us to compare the morphologies of galaxies in the Universe today with those of galaxies in the distant past. Using this definition, we calculate from the distribution shown in Figure 1 that $\simeq$89% of the star formation in the Universe today is contained in LTGs.

Using this definition, we calculate from Figure 2 that 51% of the stellar mass-density today is in ETGs. Kelvin et al. (2014a) have used the optical images of galaxies in the GAMA survey to classify the galaxies into different Hubble types. Kelvin et al. (2014b) then used these classifications to show that 34% of the stellar mass-density today is in elliptical galaxies and 37% is in S0-Sa galaxies, and so 71% of the stellar mass-density is in galaxies that would be traditionally assigned to the ETG class. The fact that our estimate
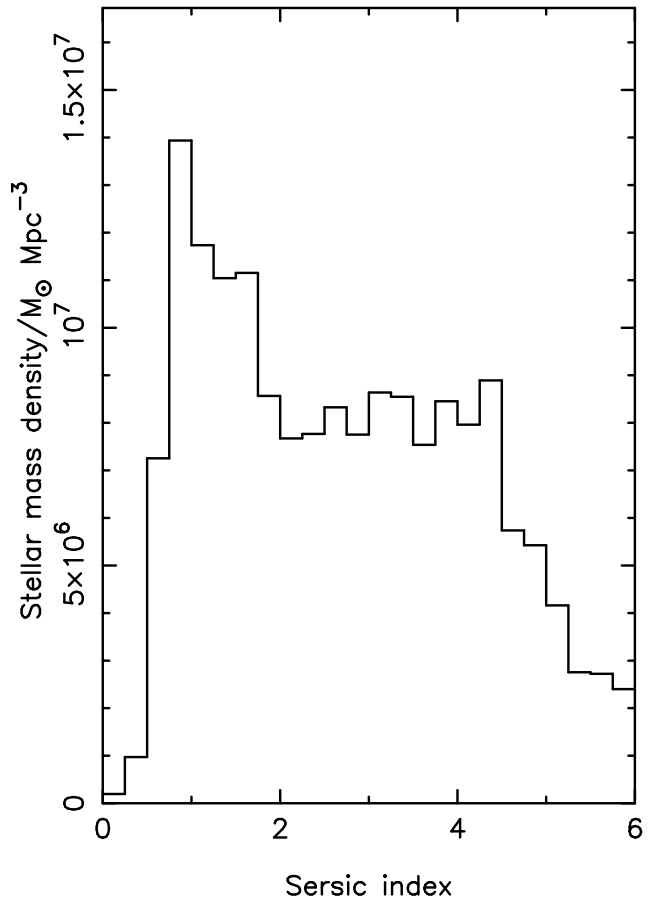
Figure 2. Stellar mass per unit comoving volume in the Universe today as a function of Sérsic index.

is lower is most likely explained by the fact that many of the Sa galaxies and and some S0s have structures that are dominated by disks (Laurikainen et al. 2010).

Another way to classify galaxies is to separate them using their colours into star-forming galaxies and 'passive' or 'quiescent' galaxies in which star formation has largely stopped (e.g. Peng et al. 2010). Although we present arguments in our accompanying paper (Eales et al. 2015) for why this classification is misleading and hides some of the physics that is going on in the galaxy population, it is true that there is a large overlap between the red passive quiescent galaxies and ETGs and between the blue star-forming galaxies and LTGs. Using the stellar mass functions for star-forming and passive galaxies given in Baldry et al. (2012), we calculate that 73% of the stellar mass-density today is in passive galaxies. The obvious explanation of our lower estimate of 51% for the fraction of the stellar mass-density that is contained in ETGs is if there is a population of passive galaxies which have structures that are dominated by disks (Van den Bergh 1976; Cortese 2012).

3 STAR FORMATION OVER THE HISTORY OF THE UNIVERSE - METHOD

3.1 The calorimetry equation

We make the assumption that all the extragalactic background radiation is due to nuclear fusion in stars. A number of theoretical arguments and observational results show that $\simeq 10\%$ of the background radiation comes from the release of gravitational energy in active galactic nuclei (Dwek and Krennrich 2013), but this should have very little effect on our final results since the absolute value of the intensity of the background is not used in our method.

The basic equation we use links the background radiation, B_ν, produced as the result of nuclear fusion in stars, with the elements that are produced by the nuclear fusion:

$$\int_0^\infty B_\nu d\nu = \int_0^{t_h} \frac{0.007\rho c^3}{4\pi(1+z)} dt \qquad (4)$$

In this equation $\rho = \rho(z)$ is the average co-moving density of elements produced by nuclear fusion in stars per unit time at a redshift z, t is cosmic time, t_H is the age of the Universe and the numerical factor, 0.007, is the fraction of the mass of hydrogen that is turned into energy when hydrogen is fused into helium. Since the products of nuclear fusion accumulate over time, this equation allows us to relate the energy dumped into the background radiation by nuclear fusion at a redshift z to the products of this nuclear fusion in the Universe today. The calorimetry equation is exact and can be derived directly from the Robertson-Walker metric, and therefore does not require any assumptions about the values of the standard cosmological parameters.

Although the equation is exact, for it to be a useful practical tool it is necessary to make some approximations. One that has been used in the past (Pagel 1997) is to assume that the density today of all the elements produced by nucleosynthesis, which includes helium, is proportional to the density today of the elements heavier than helium (the metals). In this paper, we have tried the different approach of connecting the stellar mass-density in the Universe today with the energy produced from nucleosynthesis in these stars that is now in the background radiation.

With a few assumptions, which we will discuss below, we can write the following two equations:

$$\rho_* = (1-R) \int_0^{t_h} SFR(t) dt \qquad (5)$$

$$\int_0^{t_h} SFR(t) dt = \int_0^\infty \int_0^\infty \frac{4\pi(1+z)J(z,\nu)}{0.007c^3} d\nu dz \qquad (6)$$

in which ρ_* is the current average mass-density of stars in the Universe, $SFR(t)$ is the mass of stars produced per unit volume per unit time at a redshift z, R is the fraction of that newly formed stellar mass that is subsequently ejected into the interstellar medium as the result of stellar winds (e.g. Leitner and Kravtsov 2011), $J(z,\nu)$ is the background radiation produced by objects at redshift z in a unit interval of redshift, and t_h is again the current age of the Universe.

A basic assumption that we have made to produce the first equation is that the stars formed in the Universe at a time t are still in the Universe today. This assumption seems a reasonable one since most of the mass in a stellar population is in long-lived low-mass stars.

An assumption made to produce the second equality is that all the available nuclear energy in stars has been liberated and dumped into the background radiation by the current epoch, which is obviously not true because the Sun is still shining. However, it is not a crazy assumption because most of the energy produced by a population of stars is produced by the high-mass stars, which do burn through their available nuclear energy very quickly. This is confirmed by Figure 3, where we have used models of stellar populations (Maraston 2006) to predict how the total energy that has been emitted by a single stellar population depends on age for various assumptions about the initial mass function (IMF). The figure shows that for a Salpeter or Kroupa IMF most of the energy has been emitted by 1 Gyr and the amount of energy that has been radiated (and dumped into the background radiation) increases by only $\simeq 50\%$ as the population ages from 1 Gyr to 10 Gyr.

Our main results in this paper, however, were not obtained by assuming either equality but by combining the two equations in the form of a proportionality in which we assume that the current stellar mass-density in a class of galaxies, ρ_{*c}, is proportional to the contribution of the galaxies in that class to the background radiation:

$$\rho_{*c} \propto \left[\int_0^\infty \int_0^\infty \frac{4\pi(1+z)J(z,\nu)}{0.007c^3} d\nu dz \right]_c \qquad (7)$$

The assumptions behind this proportionality are slightly different from the assumptions behind the equalities. We are now assuming that the fraction of newly formed stellar mass lost by stellar winds and that the fraction of the available nuclear energy liberated by the current epoch (see above) do not vary between galaxy classes. The second quantity is probably different between ETGs and LTGs, but we argue in §5 that the difference actually strengthens the main result in this paper.

One further assumption that is built-in to the calorimetric method is that the IMF does not vary significantly between galaxy classes. In Figure 3, we have explored the importance of this assumption by predicting the relationship between bolometric luminosity and time for different assumptions about the IMF. The figure shows that the difference between a Kroupa and a Salpeter IMF is quite small, but our results would be changed significantly if some galaxy class had a bottom-heavy IMF, because these galaxies might then contain a large mass of stars today without having contributed much radiation to the extragalactic background radiation.

3.2 The extragalactic background radiation

The extragalactic background radiation (Dole et al. 2006; Dwek and Krennrich 2013) is dominated by the radiation in two wavebands of roughly equal strength: in the optical/near-infrared, where the background peaks at $\simeq 1$-
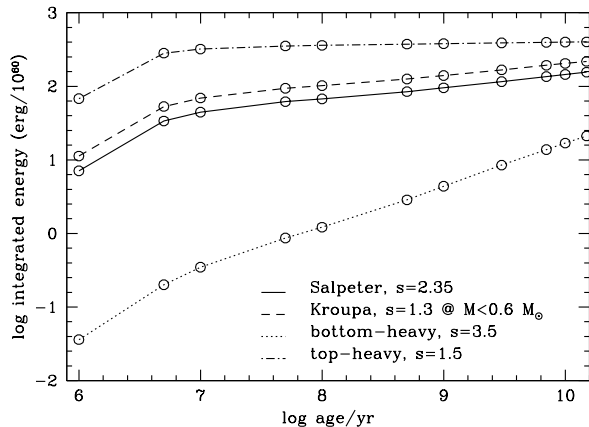
Figure 3. The total energy that has been emitted by a given age for a single stellar population with a mass of 10^{11} $M_\odot$. We have used the models of stellar populations of Maraston (2006). The different lines are for different assumptions about the stellar initial mass function. 'Kroupa' and 'Salpeter' refer to initial mass functions measured in the solar neighborhood, whereas 'top-heavy and 'bottom-heavy refer to initial mass functions with a larger proportion of high-mass and low-mass stars, respectively.

2 μm , and in the far infrared, where the background peaks at $\simeq$100-200 μm.

The far-infrared background radiation has been measured by the FIRAS and DIRBE experiments on the Cosmic Background Explorer satellite (COBE) (Fixsen et al. 1998; Dole et al. 2006; Fig. 4). In calculating the contribution of individual sources to the background (§3.3), at 160, 250, 350 and 500 μm we used the FIRAS observations of the background. The 1-σ uncertainty on the FIRAS estimate of the background is $\simeq$30%. At 100 μm we used the DIRBE measurement placed on the FIRAS flux scale (Dole et al. 2006), since the FIRAS measurements did not extend down to this wavelength.

In the optical/near-infrared, there have been three different techniques used to estimate the strength of the extragalactic background radiation: 1) estimates from integrating the galaxy counts; (2) absolute measurements of the background using the DIRBE instrument on COBE (Cambresy et al. 2001; Levenson et al. 2007); (3) searches for absorption effects in the gamma-ray spectra of distant active galactic nuclei (Dwek and Krennrich 2013). The second method would be ideal except for the systematic effects on the DIRBE near-infrared measurements from sunlight scatted by interplanetary dust. Even after a correction has been made for this scattered light, there is generally a clear relationship between the measurements of the background radiation and ecliptic latitude (Cambresy et al. 2001; Levenson et al. 2007), implying a residual contamination from interplanetary dust (reliable determinations will probably require measurements from beyond 3 A.U. from the Sun, where the

contamination from scatted light is small (Levenson et al. 2007)). These absolute measurements are 2-4 times greater than the estimate from integrating the galaxy counts, but upper limits from the gamma-ray spectra of active nuclei are generally lower than these absolute measurements, also suggesting that the DIRBE measurements are too high (Dwek and Krennrich 2013). For these reasons we have taken as our estimate of the background at 1.6 μm the integral of the deep 1.6-μm (H_{AB}) galaxy counts made with Wide Field Camera 3 on the Hubble Space Telescope (Windhorst et al. 2011).

3.3 Samples of the background radiation

To apply the calorimetry technique (§3.1), we ideally need to be able to resolve the extragalactic background radiation into individual sources. By measuring the structures of the galaxies producing the emission, we can then use equation 7 to determine the proportion of stars that have formed in galaxies with different structures.

In the southern field of the Great Observatories Origins Deep Survey (GOODS-South), we can get surprisingly close to this ideal. This field has been surveyed by the deepest survey with the Herschel Space Observatory, Herschel-GOODS (Elbaz et al. 2011; Magnelli et al. 2013) at 100 and 160 μm, close to one of the two peaks in the extragalactic background radiation. It has also been observed as part of the Cosmic Assembly Near-Infrared Deep Extragalactic Legacy Survey (CANDELS), an optical/near-infrared survey carried out with the Hubble Space Telescope with a main wavelength of 1.6 μm, close to the other peak of the extragalactic background radiation (Koekemoer et al. 2011; Guo et al. 2013). The CANDELS team has measured Sérsic indices for the galaxies detected in the survey (Van der Wel et al. 2012) from data that are well matched to the ground-based images used to estimate the Sérsic indices in our investigation of the Universe today (§2, §3.5). We now show how these surveys can be used to resolve the two peaks in the extragalactic background radiation into individual sources. Although the total area covered by the surveys of GOODS-South is only $\simeq$100 arcmin^2, we show in §4 that cosmic variance is not a significant problem, and thus that the samples of sources provided by these surveys constitute fair samples of the extragalactic background radiation.

3.3.1 Sampling the far-infrared background with the sample of Herschel sources

The public catalogue for Herschel-GOODS (H-GOODS) is available at http://hedam.lam.fr/GOODS-Herschel/. This catalogue was obtained by starting with the assumption that the sources in the 100 and 160-μm images are at a set of 'prior positions' drawn from a catalogue of sources detected at 24 μm with the Spitzer telescope, and then varying the 100-μm and 160-μm flux densities of the sources to match the observed structure in the images (Elbaz et al. 2011; Magnelli et al. 2013). The Spitzer catalogue itself was obtained in a similar way from a set of prior positions drawn from a catalogue of sources detected at 3.5 μm with the Spitzer telescope (Elbaz et al. 2011; Magnelli et al. 2013). This technique has the advantage that it produces very accurate positions for the H-GOODS sources because the 3.5-μm

sources have much more accurate positions than is possible to obtain with Herschel observations by themselves. However, it has the potential disadvantage that it could miss Herschel sources if they are not present in the prior catalogue. By comparing the H-GOODS catalogue with one obtained without using the prior catalogue, the H-GOODS team estimates that the catalogue made using the prior positions misses <4% of the sources at 160 μm (Magnelli et al. 2013). Furthermore, any missing sources will be among the fainter ones, and thus should have a negligible effect on the calorimetric technique.

The H-GOODS catalogue contains sources that were detected at 100 and 160 μm at $> 3\sigma$. Sample 1 in our analysis contains the 527 sources detected at $> 3\sigma$ at 160 μm in the region of GOODS-South also covered by the CANDELS survey. To estimate the contribution of this sample to the background radiation, we need to make measurements of the flux density at 100, 160, 250, 350 and 500 μm for every source in the sample; even if an individual detection is below the 3σ level, the result of summing the results for all the sources is often highly significant. We essentially carry out a statistical 'stacking analysis' to estimate the contribution from all the sources, even those that are not detected individually at a significant level (Marsden et al. 2009).

There are no H-GOODS images at the three longer wavelengths, so at these wavelengths we measured the flux densities of the sources from images obtained as part of the HERMES survey (Oliver et al. 2012). To measure the flux density of a source, the standard technique is to first convolve the image with the point spread function of the telescope, since this maximizes the signal-to-noise of the source. However, this is only correct if the noise on the image is uncorrelated between pixels, which is true of the instrumental noise on the HERMES images. Most of the noise on the HERMES images, however, is confusion noise, the noise due to faint submillimetre sources that are too faint to detect individually, and this noise is correlated between pixels. We did not therefore convolve the HERMES images but simply measured the flux densities from the pixel in each HERMES image that contained the position of the H-GOODS source.

The background level on a Herschel image is usually close to but not exactly zero. To estimate the residual background emission and the errors on the flux densities, we used the Monte-Carlo approach of measuring flux densities at a large number of random positions on the HERMES images without making a correction for any residual background emission. We found background levels of -0.48±0.08 mJy, -0.74±0.08 mJy and -1.1±0.08 mJy at 250, 350 and 500 μm, respectively, which we used to correct our measurements of the flux densities of the H-GOODS sources. From the Monte-Carlo simulation, the errors on these flux densities at 250, 350 and 500 μm are 6.2 mJy, 6.5 mJy and 6.2 mJy, respectively, very similar to the Herschel confusion noise at these wavelengths (Nguyen et al. 2010).

We used the 160-μm flux densities from the catalogue, but there was often not a 100-μm measurement in the catalogue. If a measurement did not exist in the catalogue, we used aperture photometry to measure the flux density from the H-GOODS 100-μm image, using an aperture with a radius equal to the full-width-half-maximum of the point spread function (6.7 arcsec). We again used a Monte-Carlo approach to estimate the residual background level

on the image and the errors on the flux densities, performing aperture photometry at a large number of random positions on the image without correcting for a residual background. We found a residual background level in our aperture of 0.3±0.03 mJy, which we used to correct the aperture photometry of the H-GOODS sources. For the H-GOODS sources for which 100-μm photometry exists in the public catalogue, we compared our measured flux densities with the catalogued flux densities to derive an aperture correction to bring our measurements on to the same flux scale as the catalogue. As a result of this comparison, we have multiplied our aperture flux densities by a factor of 1.82. From the Monte-Carlo simulation, the error on our measured flux densities is 2.4 mJy.

We estimated the contribution of the sample to the background radiation at each wavelength by adding the flux densities of the individual sources. We estimated the error on the sum by adding in quadrature the errors on the individual flux densities. The errors on the total flux density of the sources are 2%, 0.6%, 4%, 5% and 10% at 100, 160, 250, 350 and 500 μm, respectively, much less than the errors on the measurements of the background radiation at these wavelengths. Thus the errors on the percentage of the background radiation resolved by the sources are dominated by the errors on the background measurements themselves, which we assume are 30% for the measurements with FIRAS at the four longest wavelengths and 44% for the DIRBE measurement at 100 μm (Dole et al. 2006). Using these errors, our estimate of the fraction of the background contributed by the H-GOODS sample is $0.55^{+0.24}_{-0.17}$ at 100 μm, $0.67^{+0.22}_{-0.15}$ at 160 μm, $0.48^{+0.14}_{-0.11}$ at 250 μm, $0.50^{+0.15}_{-0.12}$ at 350 μm, and $0.45^{+0.14}_{-0.10}$ at 500 μm (Fig. 4). The H-GOODS team has estimated the fraction of the background resolved by the H-GOODS sources as 75% at both 100 and 160 μm (Magnelli et al. 2013). There is therefore a sizeable difference at 100 μm for which we do not know the reason.

The sample of sources detected with Herschel in the H-GOODS survey therefore constitutes a significant fraction of the background radiation but still falls significantly short, whether we use our estimates or the estimates of the H-GOODS team, from resolving all the background radiation.

3.3.2 Sampling the far-infrared background with a sample of Spitzer sources

We show now that we can actually sample a larger fraction of the far-infrared background using a sample of sources detected at 24 μm in the GOODS-South region by the Spitzer Space Telescope. This sample (sample 2) consists of 1557 sources detected at 24 μm in the same area of GOODS-South that is covered by CANDELS. We measured the flux densities of each of these sources at 250, 350 and 500 μm from the HERMES images in the same way as for sample 1. At 100 and 160 μm, we used for preference the flux densities given in the H-GOODS public catalogue. If there was not a 100-μm measurement in the public catalogue, we carried out aperture photometry on the H-GOODS 100-μm image in exactly the same way as for sample 1. For sample 2 this was often also necessary at 160 μm. In this case we measured a 160-μm flux density from the H-GOODS 160-μm image through an aperture with a radius equal to the full-width-half-maximum of the point spread function (11.0 arcsec). We

used the Monte-Carlo method of performing aperture photometry at a large number of random positions on the H-GOODS 160-μm image to estimate the residual background level in this aperture of 2.0±0.07 mJy, which we allowed for in the measurements of the flux densities of the H-GOODS sources. By comparing our measured flux densities with the ones in the catalogue, where they exist, we derived a correction factor of 2.0, by which we multiplied our aperture flux densities to bring them on to the same flux scale as the catalogue. From the Monte-Carlo simulation, our estimate of the error in our 160-μm flux densities is 5.6 mJy.

For sample 2, the error in the total flux density of the sources is 5%, 7%, 4%, 5% and 8% at 100, 160, 250, 350 and 500 μm, respectively, which are again much less than the errors in the level of the backround. Using 30% as the error in the FIRAS measurements of the background at the four longest wavelengths and 44% as the error in the DIRBE background measurement at 100 μm, we calculate that the sources in sample 2 compose $0.67^{+0.29}_{-0.20}$ of the background radiation at 100 μm, $0.90^{+0.27}_{-0.21}$ at 160 μm, $0.80^{+0.24}_{-0.19}$ at 250 μm, $0.89^{+0.27}_{-0.21}$ at 350 μm, and $0.90^{+0.27}_{-0.21}$ at 500 μm. Given the uncertainties, the combined far-infrared flux density from sample 2 is fully consistent with the far-infrared background radiation over this range of wavelengths. The sources in this sample therefore represent a fair sample of the extragalactic background radiation in one of its two main peaks.

3.3.3 *Sampling the optical/near-infrared background with the HST*

The other peak in the extragalactic background radiation is in the optical/near-infrared waveband. As our sample of this peak (sample 3) we use the 8488 galaxies detected by CANDELS with $H_{AB} < 24.5$ in the GOODS-South field. We have used this photometric band because its central wavelength ($\simeq 1.6$ μm) is close to the peak of the optical/near-infrared background. We have used the magnitude limit because galaxies fainter than this do not generally have reliable measurements of the Sérsic index (Van der Wel et al. 2012). This sample constitutes $\simeq 94$% of the extragalactic background radiation at 1.6 μm. The high value is the result of our assumption that the extragalactic background radiation at this wavelength is given by the integral of the galaxy counts (§3.2); since the slope of the galaxy counts flattens at $H_{AB} \simeq 21$ (Windhorst et al. 2011), the fraction of the background radiation produced by galaxies with $H_{AB} < 24.5$ is very high. As long as there is not a substantial contribution to the extragalactic background radiation from starlight that is not detected in even the deepest exposures with the HST (§5), sample 3 constitutes a fair sample of the extragalactic background radiation in its second peak.

We have included all the data for samples 1 and 2 that was used in this paper in on-line tables. The tables includes the positions of the Herschel and Spitzer sources, the flux densities at the five Herschel wavelengths, the spectroscopic and/or photometric redshifts of the sources, the positions of the counterparts on the HST images (§3.4) and the Sérsic indices of the counterparts (§3.5).
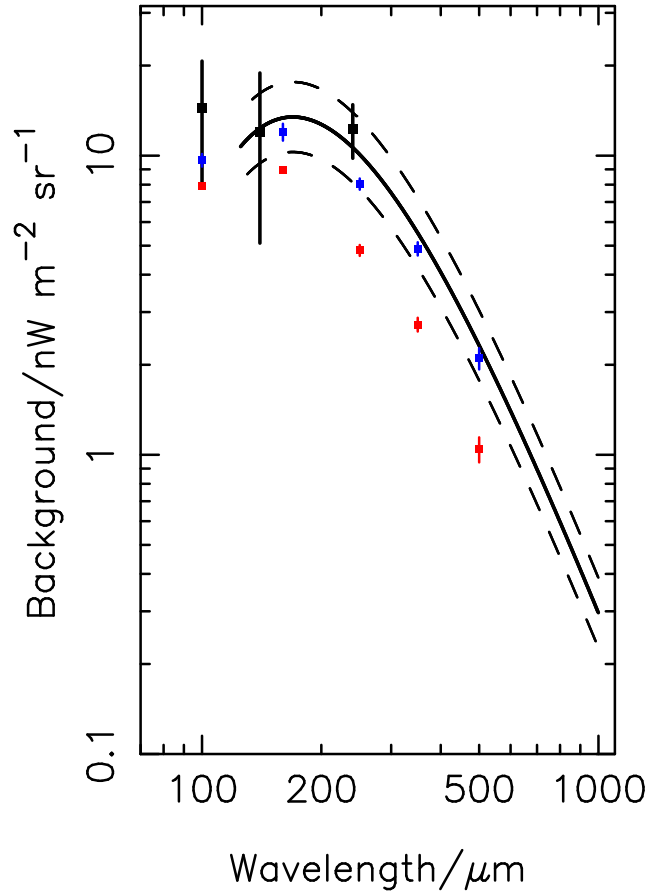
Figure 4. The extragalactic far-infrared background radiation plotted against wavelength, and our estimates of the contribution to this background from the samples described in this paper. The heavy solid line shows the measurement of the background with the FIRAS experiment on COBE (Fixsen et al. 1998), with the light dashed lines showing the ±1σ errors on the background. The black points show the measurements made by the DIRBE experiment on COBE (Dole et al. 2006). The red points show our measurements of the contribution to the background radiation from the sources individually detected at 160 μm by the H-GOODS survey (sample 1). The blue points show our measurements, using the Herschel images of GOODS South, of the contribution to the background radiation from the sources that were originally detected at 24 μm with Spitzer (sample 2).

3.4 Identifying the counterparts to the Herschel and Spitzer sources

There are measurements of the Sérsic index for all the galaxies in sample 3 by the CANDELS team (Van der Wel et al. 2012). However, for the other two samples, before we can consider the structures of the galaxies producing the far-infrared emission, we need to identify these galaxies.

The positions of the sources in samples 1 and 2 are ultimately based on observations with the Spitzer Space Telescope at 3.5 μm, which have an angular resolution (FWHM) of 1.7 arcsec. The accuracy of the positions should therefore be <1 arcsec, and we have made the assumption that any genuine counterpart to a Herschel/Spitzer source on the CANDELS H-band (1.6 μm) image must lie within 1.5 arcsec of the position of the source.

To assess the probability of a possible counterpart on

the CANDELS image within 1.5 arcsec of the position of the Herschel/Spitzer source being there by chance, we follow the frequentist technique commonly used in far-infrared astronomy of calculating a statistic, S, for the counterpart, defined as the number of CANDELS galaxies brighter than the 1.6-μm flux density of the potential counterpart that are expected by chance to lie closer to the Herschel/Spitzer position than the potential counterpart (Dye et al. 2009). If there was more than one possible counterpart within 1.5 arcsec, we chose the one with the lowest value of S as the most likely counterpart. We estimated the probability, P, of obtaining such a low value of S, given the null hypothesis that there is no relation between the CANDELS galaxies and the Herschel/Spitzer sources, by the Monte-Carlo approach of measuring S for a large number of random positions on the image. Sample 1 contains 527 sources and we found possible counterparts within 1.5 arcsec for 526. We estimated the number of counterparts that are there by chance by summing P for the 526 counterparts, which is 3.0. Therefore <1% of the counterparts are likely to be spurious. Sample 2 contains 1557 sources and we found possible counterparts within 1.5 arcsec for 1537. In this case, the sum of P is 9.9, again showing that <1% of the counterparts are likely to be spurious.

From a formal statistical point of view, there is no reason why this frequentist technique should produce any biases. However, one might worry that, because the flux at 1.6 μm is used in the calculation, the technique is biased against highly obscured dusty galaxies, the kind that one might expect to be far-infrared sources. However, an investigation shows that this is not the case. In sample 1, of the 527 160-μm sources, there were 92 cases where there was more than one potential HST counterpart within 1.5 arcsec. In only 5 of the 92 cases was there an object fainter than the selected counterpart but closer to the Herschel position. A final argument that the method is reliable is that 77% of the selected counterparts lie within 0.2 arcsec of the position of the Herschel source, whereas our Monte-Carlo analysis shows that the distribution of offsets for random positions reaches a maximum at >1 arcsec.

3.5   The Sérsic indices of the CANDELS galaxies

In this section we consider whether any systematic errors might arise from comparing the Sérsic indices of the H-ATLAS galaxies (§2) with those measured for the galaxies detected in CANDELS.

The Sérsic indices for the H-ATLAS sources were measured from the r-band (0.62 μm) images from the Sloan Digital Sky Survey (SDSS) (Kelvin et al. 2012). The Sérsic indices for the H-GOODS galaxies were measured from H-band (1.6 μm) images from the CANDELS HST programme (Van der Wel et al. 2012). The median redshift of the H-ATLAS galaxies is 0.07, whereas most of the H-GOODS galaxies lie at $z > 1$ (§4). For these redshifts, the HST images of the H-GOODS galaxies (angular resolution of 0.17 arcsec) and the SDSS images of the H-ATLAS galaxies (angular resolution $\simeq$1 arcsec) give almost exactly the same physical resolution, $\simeq$1.3 kpc. The r-band image of a galaxy at $z = 0$ and the H-band image of an H-GOODS galaxy at $z = 1.6$, which is fairly representative of the H-GOODS redshift distribution (§4), correspond to the same rest-frame

wavelength. The similarity of the rest-frame wavelengths ensures that there should be no biases created by the small changes that are evident when Sérsic indices are measured at different wavelengths (Kelvin et al. 2012). The one slight mismatch is in the sensitivity to surface brightness for the two datasets. The HST image of an H-GOODS galaxy at $z = 1.6$ has $\simeq$1 mag less surface-brightness sensitivity than the SDSS image at the same rest-frame wavelength of a galaxy at $z = 0$, and the difference increases at $z > 1.6$. Van der Wel et al. (2012) have investigated the effect of the signal-to-noise on the CANDELS images on the measured value of the Sérsic index, concluding that there is little bias down to $H_{AB} = 23.0$ but that by $H_{AB} = 24.0$ galaxies with high values of the Sérsic index ($n > 3$) will have measured values that are lower than the true values by 25% (see their Table 3). Therefore, some of the fainter objects in our high-redshift sample may have measured Sérsic indices that are too low.

3.6   Practical application of the calorimetry technique

Subject to the assumptions discussed in §3.1, equation 7 shows that the stellar mass-density in the Universe today associated with the star-formation in the i'th source in a fair sample of the background radiation is proportional to $J_i(1 + z_i)$, in which z_i is the redshift of the galaxy and J_i is the contribution of this galaxy to the extragalactic background radiation [1]. Therefore, given estimates of J_i and z_i for all the galaxies in a fair sample of the background radiation, it is straightforward to estimate the stellar mass-density in the Universe today produced as the result of the formation of stars over the history of the Universe. Given measurements of the Sérsic index for each galaxy in a sample, it is also straightforward to estimate how the stellar mass-density today *depends on the Sérsic index of the galaxy in which those stars were formed.* It is important to note that these stars may well now be in a galaxy very unlike that in which the stars were formed, either as the result of the merging of galaxies or some other process that has transformed the structure of the galaxy.

Since the flux densities of individual galaxies are often detected with very low signal-to-noise or are even negative, we calculated J_i in both the optical/near-infrared and the far infrared using the following formula, which provides a robust estimate in this situation:

$$J_i = \sum_j F_{ij} \Delta \nu_j \qquad (8)$$

In this formula F_{ij} is the flux density of the i'th galaxy in the j'th band and $\Delta \nu_j$ is the frequency range associated with that band. We adopted the very simple approach of assuming that the boundaries between two bands, for example

---

[1] There is no causal association, of course. We are using the samples to represent the energy generated by nucleosynthesis over the history of the Universe, but the starlight we are detecting in the early Universe has no causal connection with the stars we see today. We are implicitly assuming the cosmological principle that any region of the Universe looks like any other.

the Herschel bands centred at 100 and 160 μm, lie equidistant in log(frequency) between the two central wavelengths. For samples 1 and 2, we calculated J_i from the measured flux densities of each galaxy at 100, 160, 250, 350 and 500 μm. For sample 3, we calculated J_i from measurements of the flux density in the following photometric bands (Guo et al. 2013): U-band, ACS F606W, ACS F814W, WFC125W, WFC160W, IRACB1 and IRACB2.

For redshifts we used, in order of preference, spectroscopic redshifts, the photometric redshifts that form part of the H-GOODS public data release and the catalogue of photometric redshifts for the CANDELS galaxies (Li-Ting et al. 2014).

After losing $\simeq 1\%$ of the sources for which we could not find a counterpart on the CANDELS image, samples 1 and 2, contain 526 and 1537 galaxies, respectively. We removed $\simeq 10\%$ of the galaxies in each sample for which the flag for the Sérsic measurement (Van der Wel et al. 2012) implies the measurement is not reliable, leaving 467 and 1358 galaxies in samples 1 and 2, respectively. Of the galaxies that are left, 352 (75%) in sample 1 and 903 (66%) in sample 2 have spectroscopic redshifts; for the remaining galaxies we used the photometric redshifts.

In the optical/near-infrared, sample 3 contains 8488 objects with $H_{AB} < 24.5$. The small size of the field means that there is the potential for effects due to cosmic variance (§4). These effects will be largest at low redshifts, and indeed there are a large number of galaxies at $z \simeq 0.05$. To minimize these effects we excluded 123 galaxies with redshifts < 0.06. We also excluded 15 very bright objects with Sérsic indices of < 0.6, which are probably stars or quasars. Of the remaining objects, we eliminated $\simeq 20\%$ for which the flag implies there is not a reliable measurement of the Sérsic index (Van der Wel et al. 2012). Of the remaining 6753 galaxies, 2482 (37%) have spectroscopic redshifts, and for the others we used the photometric redshifts.

4   RESULTS

Figure 5 shows the redshift distributions of the three samples. Since GOODS-South is such a small field, an obvious concern is whether it is a fair sample of the Universe and, in particular, of the extragalactic background radiation. We estimated the cosmic variance for the three samples using the on-line calculator described by Treventi and Stiavelli (2008). Using a mean redshift of 1.0 and a redshift interval of 2.0, we estimate that cosmic variance leads to errors in the total numbers of sources in samples 1, 2 and 3 of 7, 6 and 5%, respectively. Therefore, the samples as a whole are likely to be fair samples of the overall background radiation. When we apply the on-line calculator to the individual redshift bins, which have a width of 0.2 in redshift, we find that the uncertainty in the number of sources in each redshift bin is $\simeq 30\%$ for samples 1 and 2 (left-hand panel of Figure 5). Hence the lumpy nature of the redshift distributions in Fig. 5 is probably the result of large-scale structure. Note that there are well-known over-densities in GOODS-South at $z = 0.66$ and $z = 0.735$ (Adami et al. 2005).

Using the values of $J_i(1 + z_i)$ and equation 6, we have estimated the star-formation history of the Universe: the star-formation rate per unit comoving volume as a func-

tion of redshift. Figure 6 shows the star-formation history derived from the data for the three samples. Not surprisingly, at a given redshift the star-formation rate for sample 2 is higher than for sample 1 because the sources in sample 2 comprise a larger fraction of the background radiation. The star-formation histories derived from all three samples are rather noisy, the consequence of large-scale structure, but all three star-formation histories peak somewhere in the redshift range $1 < z < 3$, consistent with the results of previous attempts to derive the Universe's star-formation history (e.g. Hopkins and Beacom 2006).

Figure 7 shows the estimates from the three samples for the relationship between the stellar mass-density in the Universe today and the Sérsic index of the galaxy in which those stars contributing to that mass-density were formed. We showed in §2 that in the Universe today 51% of the stellar mass density is in ETGs, which we empirically defined as galaxies with a Sérsic index > 2.5. If the structures of these galaxies have not changed between the time the stars now in them were formed and the current epoch, we would expect Figure 7 to look very like Figure 2. On the contrary, the distributions for all three samples are strikingly similar to Figure 1, which showed how the star-formation rate in the Universe today depends on the Sérsic index of the galaxy in which the those stars are being formed. Figure 1 showed, not unexpectedly, that, today, most stars form in LTGs. Figure 7 shows that this has always been true, that even though most stars today are in ETGs, most stars formed in LTGs.

We can quantify this very easily by measuring the proportions of the distributions in Figure 7 that lie on either side of the $n = 2.5$ dividing line. The result from both the samples of the far-infrared background, samples 1 and 2, is that $\simeq 87\%$ of the stellar mass that is in the Universe today must have formed in LTGs. The result from the sample of the optical/near-infrared background, sample 3, is that $\simeq 79\%$ of the stellar mass today was formed in LTGs. To assess the importance of the measurement errors for the Sérsic indices on these estimates, we carried out a bootstrap analysis for the smallest sample, sample 1. We generated 1000 artificial versions of sample 1, using a random-number generator to produce from the measured Sérsic index and measurement error for each galaxy a new 'measurement' in each sample for that galaxy. From these 1000 samples, we estimate the statistical uncertainty in our estimate of 0.87 for the fraction of the stellar mass-density formed in LTGs as only 1.9×10^{-6}. We discuss other more important sources of error in the following section.

Taking an average of the results for the two peaks in the background radiation, which is reasonable since they have roughly equal strength, our results imply that $\simeq 83\%$ of the stellar mass today was formed in LTGs. This is much higher than our estimate of 49% for the percentage of the stellar mass-density that is today in LTGs. The big difference in the values implies that the morphological transformation of galaxies must be an important part of galaxy evolution.

5   DISCUSSION

The importance of the calorimetric approach is that it produces a quantitative measurement of the stellar mass-density that has formed in galaxies with different morphologies
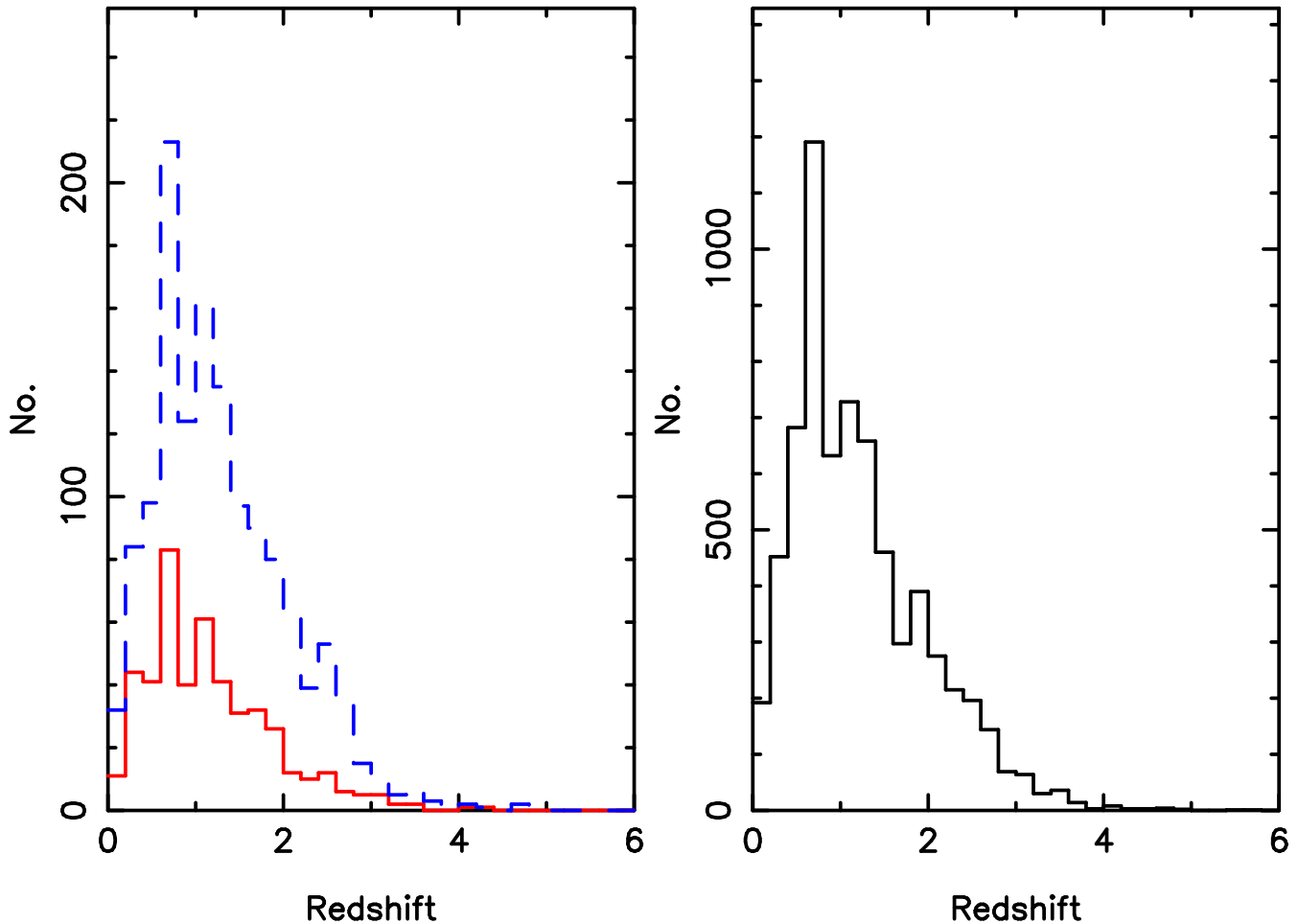
Figure 5. Redshift distributions of the samples of the far-infrared background radiation (left) and the optical/near-infrared background radiation (right). The red line in the left-hand panel shows the redshift distribution for the sample of sources detected by Herschel (sample 1) and the blue dashed line shows the redshift distribution for the sample of sources detected with Spitzer (sample 2).

which covers all cosmic epochs and galaxy masses, since the extragalactic background radiation contains all the energy ever emitted as the result of nuclear fusion in stars. The calorimetric technique, if there are no practical problems—we will discuss some of the possibilities next—makes it impossible for star formation to hide anywhere.

One fundamental problem we can do nothing about is that the method is based on the assumption of a universal initial mass function. As we showed in §3.1, a population of stars that are formed with a bottom-heavy initial mass function may lead to a large stellar mass-density in the Universe today but not have dumped much radiation into the extragalactic background radiation.

A less fundamental problem, but one we can still do nothing about, is that the uncertainties on the absolute values of the extragalactic background radiation still leave some places for star formation to hide; if the far-infrared background is at the upper end of the range set by the errors (Fig. 4), or if the optical/near-infrared background has a component that is not detected in the deep HST surveys, our samples may comprise substantially smaller percentages of the background radiation than we have estimated.

Third, we have missed some of the energy produced by nucleosynthesis in stars because we have only considered the

background radiation over two limited ranges of wavelength around each of the two peaks in the background radiation (§4). This will only be a problem if the galaxies comprising the missing part of the background radiation have systematically different morphologies from the galaxies in our samples of the two peaks. This is possible, but seems unlikely because the two peaks are separated by a factor of $\simeq 100$ in wavelength, yet the morphological makeup of the galaxies in the samples of the two peaks are quite similar (compare the right and left panels of Fig. 7).

Fourth, there is the issue that for any population of stars, not all the available nuclear energy will have been dumped into the extragalactic background radiation by the current epoch (§3.1, §4). ETGs generally have older stellar populations than LTGs (Kennicutt 1998) and thus should have dumped a larger fraction of the total available nuclear energy into the background radiation by the current epoch, and so if there is a systematic bias it will be in the sense that samples of the extragalactic background radiation preferentially contain ETGs. Therefore, this may have led us to underestimate the true difference beween the fraction of the stellar mass-density that is in LTGs today and the fraction of the total stellar mass-density that was formed in LTGs.

Fifth, there is the issue that ETGs with lower stellar
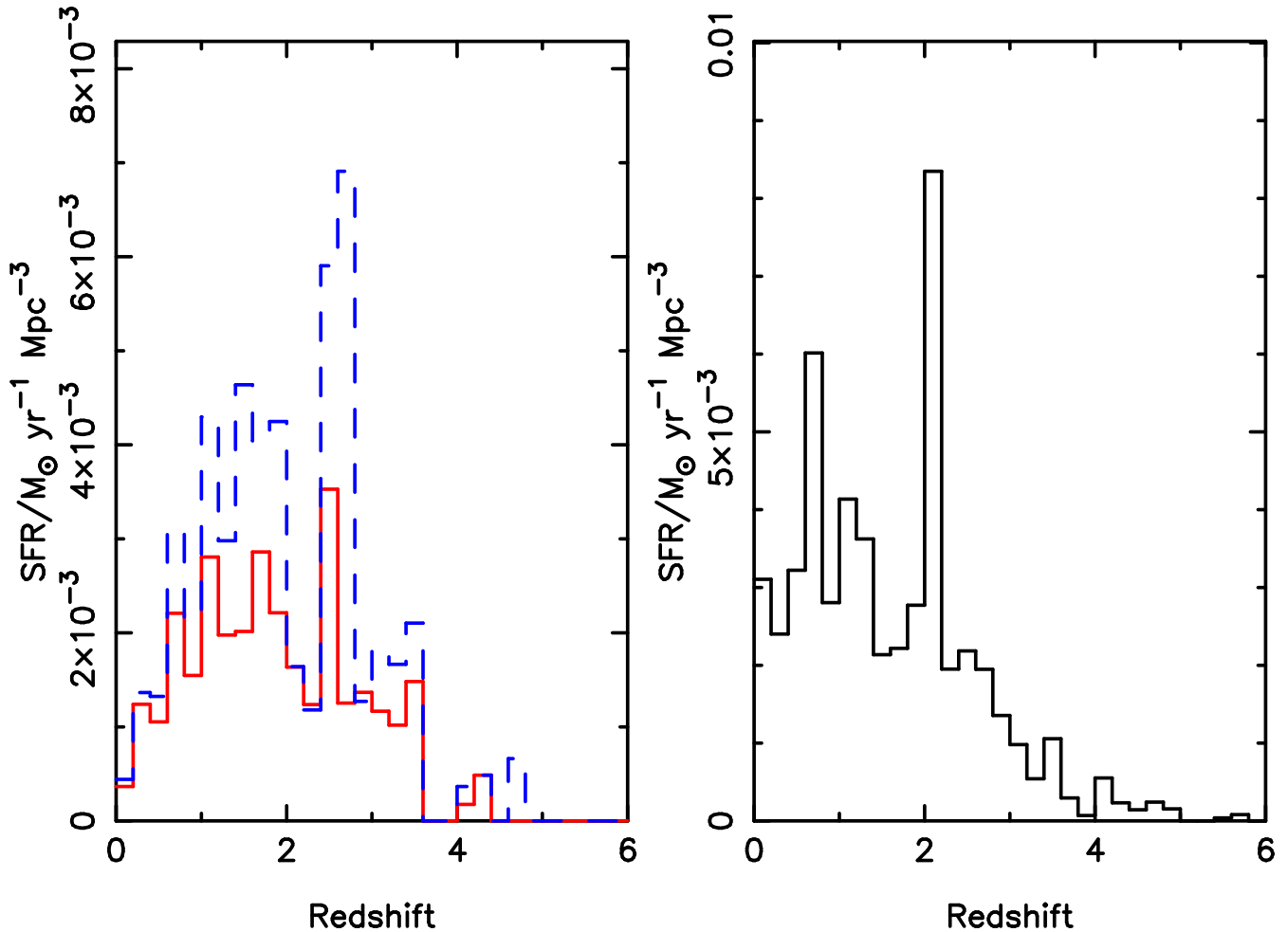
Figure 6. Star-formation density (star-formation rate per unit comoving volume) derived by applying the calorimetric technique to the far-infrared background radiation (left) and to the optical/near-infrared background (right). In the left-hand panel, the red line shows the results for sample 1 and the blue line the results for sample 2.

masses, such as dwarf elliptical galaxies, do have low values of the Sérsic index (Graham and Guzman 2003). Allen et al. (2015) have used MAGPHYS to estimate the stellar masses of the H-GOODS galaxies using the photometry provided in Guo et al. (2013). Figure 8 shows the distribution of stellar masses for the HGOODS galaxies, which shows that their low values of the Sérsic index cannot be attributed to low stellar masses.

With a few caveats, the most important of which is probably our assumption of a universal initial mass function, our conclusion that most stars form in LTGs but most of the stellar mass-density today is in ETGs seems secure. A necessary implication of our conclusion is that there must have been some process that transformed the morphologies of many galaxies from the LTG class to the ETG class after most of the stars in each galaxy had been formed.

However, before we consider the mechanisms that might cause this major morphological transformation of the galaxy population, we have to consider what our LTG/ETG classification means when we apply it to galaxies at high redshift. At low redshift, an LTG is generally a galaxy whose structure is dominated by a disk and an ETG is a galaxy which has a prominent bulge or spheroid. A common assumption

is that this must also be true at high redshift, which is part of the reason for the conclusion from HST imaging studies that star-forming galaxies at high redshift have structures dominated by disks (e.g Wuyts et al. 2011; Bruce et al. 2012). However, there is at least one way in which galaxy evolution might have made this an unsafe assumption. The bulges of low-redshift spiral galaxies often have Sérsic indices < 2.5 (Balcells et al. 2003). Therefore, one possibility we have to consider is that the high-redshift galaxies are naked spheroids, which will subsequently accrete a disk and grow into the spiral galaxies we see around us today.

There are two main arguments against this idea. The first is the circumstantial argument that most of the high-redshift galaxies do actually look like they have disks. In Figure 9 we have shown the CANDELS images in the H_{AB}-band (1.6 μm) of the galaxies in sample 1 [2]. There are very

[2] We have chosen sample 1 rather than sample 2, despite the fact the latter constitutes statistically a larger fraction of the background radiation, because we can be more confident that individual galaxies in sample 1 are emitting far-infrared radiation since each was detected by the Herschel Space Observatory at 160 μm.
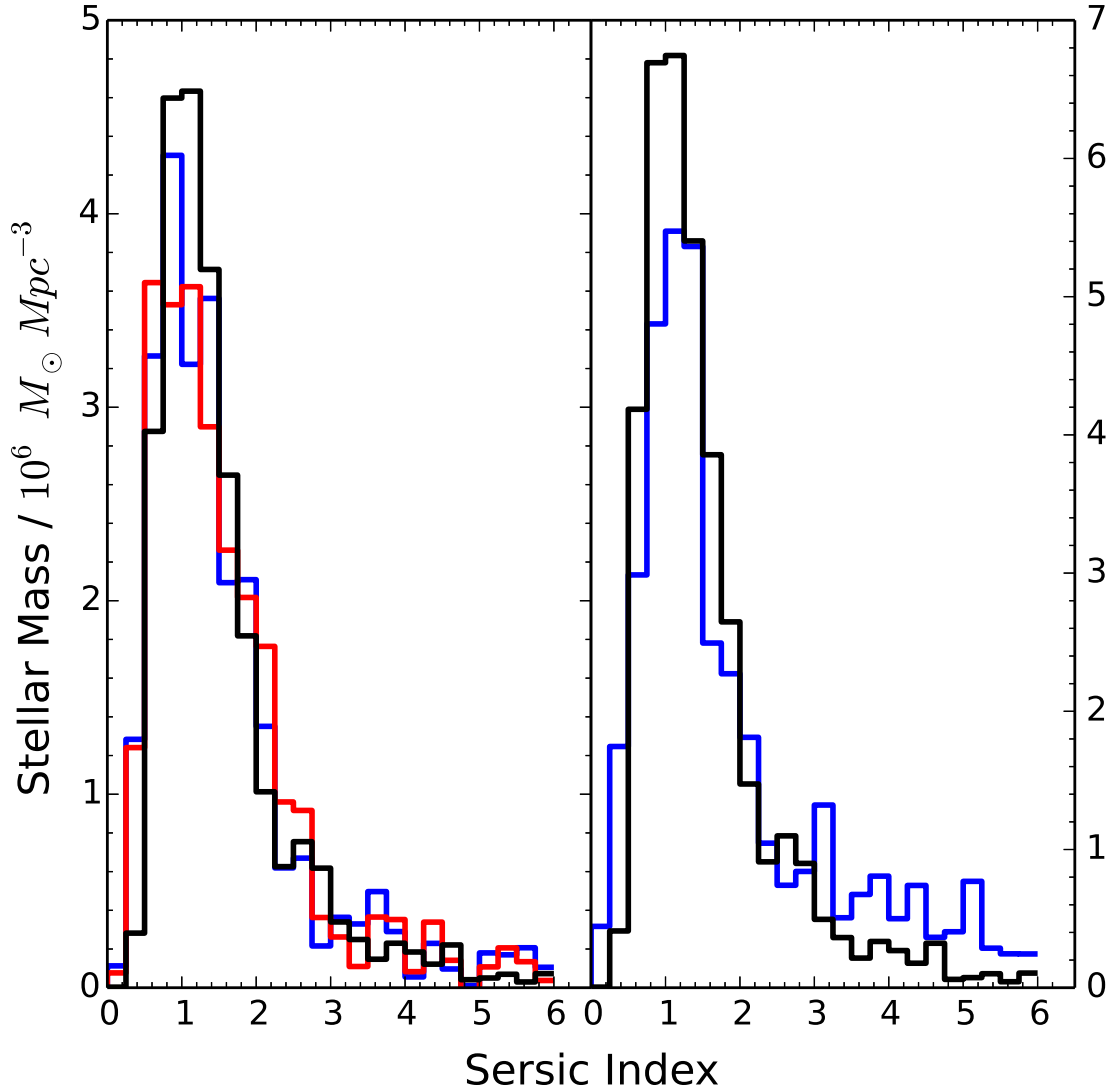
Figure 7. The relationship between the stellar mass-density in the Universe today and the Sérsic index of the galaxy in which the stars were formed. The two panels show the results for our calorimetric samples of the far-infrared (left) and optical/near-infrared (right) backgrounds; the blue and red line in the left-hand panel show the results for samples 1 and 2, respectively, and the blue line in the right-hand panel shows the results for sample 3. The histogram for sample 1 in the left-hand panel has been normalised so that the area under it is the same as for sample 2. In both panels the black line shows the star-formation rate in the Universe today as a function of Sérsic index (Fig. 1) normalized so that it encloses the same area as the other histograms. Note the absence of a peak at $n = 4$, which should be present if stars that are currently in elliptical galaxies were born in galaxies with the same structures.

few galaxies in this sample, even ones with high values of the Sérsic index, for which there is not some sign of a disk on the HST image.

The second argument that our operationally-defined LTGs are similar to the disk-dominated systems in the Universe today comes from the results of a different technique for investigating the morphologies of high-redshift galaxies. A number of groups have inferred the morphological composition of a high-redshift sample by modelling the distribution of ellipticities of the images of the galaxies (e.g. Ravindranath et al. 2006; Van der Wel et al. 2014). Using

a large sample of $\simeq 40,000$ star-forming galaxies from CANDELS, Van der Wel et al. (2014) show that the distribution of ellipticities of star-forming CANDELS galaxies with $1.5 < z < 2.0$ and stellar masses $> 10^{10} \ M_\odot$ can be reproduced by a model in which $\simeq 75\%$ of the galaxies are disks, with almost all the remaining objects having a spheroidal structure. Both studies also found a significant population with highly elongated structures which could not be explained by the predicted fraction of highly edge-on disks, but in the study of the CANDELS sample these highly elongated galaxies are found below a stellar mass of $10^{10} \ M_\odot$,
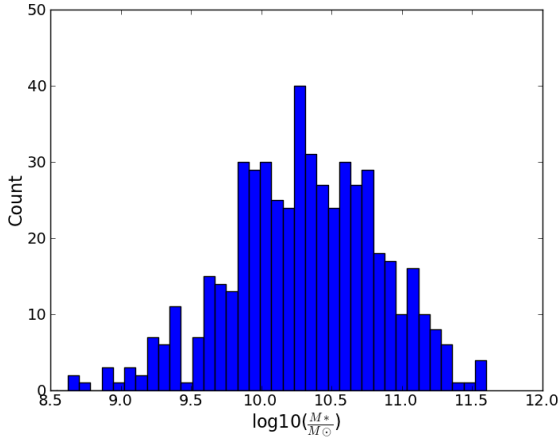
Figure 8. Estimates of the stellar masses of the galaxies in sample 1 from modeling their spectral energy distributions with MAGPHYS (Allen et al. in preparation).

whereas most of the galaxies in our sample 1 have higher stellar masses (Fig. 8).

Despite these arguments, we can not rule out the idea that high-redshift LTGs are physically a different type of object to the disk-dominated galaxies in the local Universe, especially as high-redshift galaxies are physically smaller (Bruce et al. 2014) and have more turbulent velocity fields (Genzel et al. 2014). **However, even if the LTGs at high redshift are physically distinct from the disk-dominated objects that are LTGs at low redshift, this does not eliminate the need to find a mechanism for transforming LTGs into ETGs.** Suppose, for example, the high-redshift LTGs are naked spheroids. There still needs to be some mechanism to turn these into ETGs, since the obvious evolutionary process, the growth of a disk around the spheroid, would still produce a low-redshift galaxy with $n < 2.5$.

Before we turn to the mechanisms that might have caused this morphological shift, it is worth pointing out that our result is a statistical result and does not mean there can not be evolutionary mechanisms that either leave the morphologies untouched or work in the other direction. For example, Graham et al. (2015) have argued that the compact passive galaxies discovered at high redshift a decade ago (Daddi et al. 2005; Trujillo et al. 2006) are the ancestors of the bulges of low-redshift S0 or spiral galaxies, and that the evolution from one into the other will occur by the growth of a disk around the naked bulge - the same mechanism that we considered above for the general galaxy population. It is possible that this morphological transformation occurs, but the following argument implies that its scale is much less than the morphological transformation from LTGs to ETGs implied by the calorimetry results.

Graham et al. have estimated that the descendant population in this transformation, the spirals and S0s in the Universe today with bulge structures very similar to the structures of the compact passive galaxies at high redshift, have stellar masses of $\simeq 10^{11}\ M_\odot$ and a volume density of $3.5 \times 10^{-5}\ Mpc^{-3}\ dex^{-1}$, although this is strictly only a lower limit. The stellar mass-density in the descendant pop-

ulation is thus $\simeq 3.5 \times 10^6\ M_\odot\ Mpc^{-3}$. However, the total stellar mass-density in the Universe today (the integral of the distribution in Fig. 2) is $1.9 \times 10^8\ M_\odot\ Mpc^{-3}$, approximately 50 times larger. Thus this evolutionary channel may exist, but the morphological change from LTGs to ETGs revealed by the calorimetry results involves a much larger fraction of the current stellar mass-density.

We now consider the mechanisms that might have produced this major change, and from now on we assume that the LTGs at high redshift are disk-dominated galaxies. Of the theoretical ideas for morphological transformation that were discussed in §1, two are clearly consistent with the idea that LTGs predate ETGs: 1) the idea that ETGs are formed by the merger of two LTGs (Toomre 1977); (2) the idea that the spheroid in a galaxy is built up by the rapid motion of star-forming clumps towards the centre of the galaxy (Noguchi 1999; Bournaud et al. 2007; Genzel et al. 2011, 2014).

The evidence from HST imaging that star-forming galaxies at all redshifts are LTGs and passive galaxies are ETGs (Bell et al. 2004a; Wuyts et al. 2011; Bell et al. 2012; Bruce et al. 2012; Buitrago et al. 2013; Szomoru et al. 2013; Tasca et al. 2014) is evidence that the process responsible for the morphological transformation is the same one that is responsible for quenching the star formation in a galaxy (Bell et al. 2012). This evidence favours the second of the ideas above, since it provides a clear explanation for both morphological transformation and quenching. Additional circumstantial evidence for this conclusion is that most ETGs in the Universe today contain some evidence of a residual disk once you look closely enough (Krajnovic et al. 2013).

To explain our result, the morphological transformation of an LTG must have occurred after most of the stars in the galaxy had formed. The average star-formation rate in the Universe dropped rapidly over the redshift range $1 > z > 0$ (Hopkins and Beacom 2006; Eales et al. 2015), suggesting that this redshift range may have been the one in which morphological transformation was most active. Two other results point in this direction. First, many studies have shown that $\simeq 50\%$ of the stellar mass in 'passive galaxies', which overlaps substantially with ETGs, was formed since $z \simeq 1$ (Chen et al. 2003; Bell et al. 2004; Faber et al. 2006). Second, Tasca et al. (2014) have observed a gradual decline in the optical emission from disks over this redshift range. If this is the critical redshift range, the high-resolution wide-field surveys with Euclid will be crucial for investigating the transformation process.

6   CONCLUSIONS

In this paper, we have tried to quantify the importance of morphological transformation in galaxy evolution. We have used the operational definition that an early-type galaxy (ETG) is one with a Sérsic index > 2.5 and a late-type galaxy (LTG) is one with a Sérsic index of <2.5. Using this definition, we have obtained the following two observational results:

1 We have used the results of the Galaxy and Mass Assembly project and the Herschel Astrophysical Terrahertz Large-Area Survey to show that in the Universe today 51%

of the stellar mass-density is in ETGs but 89% of the rate of production of stellar mass-density is occurring in LTGs.

2 The extragalactic background radiation contains all the energy generated by nuclear fusion in stars since the Big Bang. We have resolved the background radiation into individual galaxies using the deepest far-infrared survey with the Herschel Space Observatory and a deep near-infrared/optical survey with the Hubble Space Telescope (HST). Using measurements of the Sérsic index of these galaxies derived from the HST images, we estimate that $\simeq 83\%$ of the stellar mass-density formed over the history of the Universe occurred in LTGs.

Our second result is subject to a number of caveats, the most importance of which is that our calorimetric method is based on the assumption of a universal initial mass function. Subject to these caveats, the difference between the fraction of the stellar mass-density today that is in LTGs and the fraction that was formed in these galaxies implies that there must have been a major morphological transformation of LTGs into ETGs after the formation of most of the stars.

Our remaining conclusions are less certain. Since the star-formation density started to decline at $z \simeq 1$ and since there is evidence for the build-up of stellar mass-density in passive galaxies since that redshift, it seems likely that the morphological transformation from LTGs to ETGs occurred over the redshift range $0 < z < 1$. If this conclusion is true, a high-resolution investigation of the morphologies of galaxies over this redshift range, such as will be possible with Euclid, will be important for determining the process that is responsible for the transformation.

The fact that HST imaging programmes show that star-forming galaxies at all redshifts are dominated by disks, while passive galaxies have spheroidal structures, implies there is a single process responsible both for the morphological transformation and the quenching of galaxies. This favours models such as those in which the growth of a bulge in the centre of a disk shuts down star formation by stablising the disk against gravitational collapse.
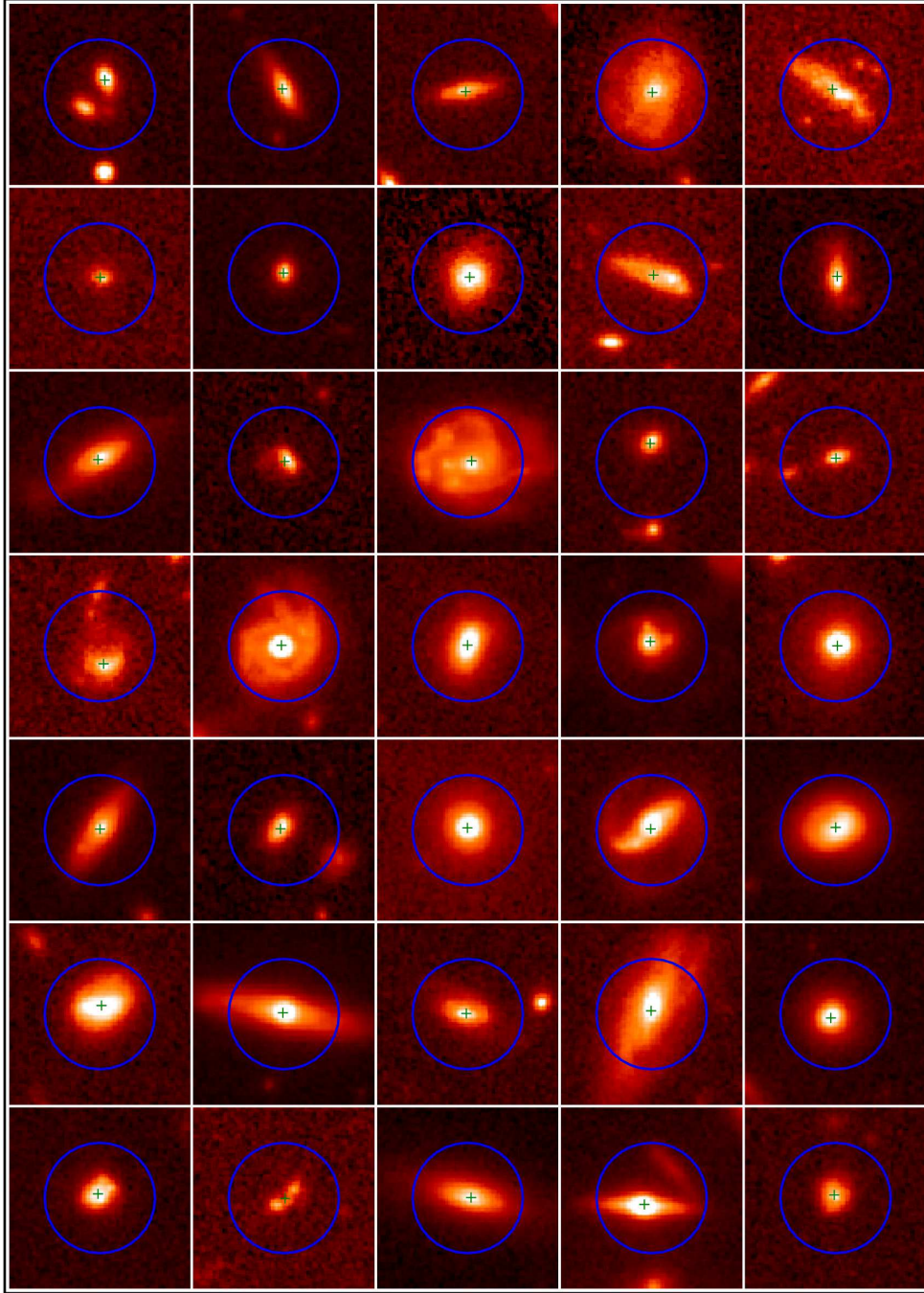
REFERENCES

Abazajian, K. et al. 2009, ApJS, 182, 543
Adami, C. et al. 2005, A.&A. 443, 805
Balcells, M., Graham, A.W., Dominguez-Palmero, L. & Peletier, R.F. 2003, ApJ, 582, L79
Baldry, I.K. 2008, A&G, 49, 25
Baldry, I.K. et al. 2012, MNRAS, 421, 621
Bell, E.F. et al. 2004a, ApJ, 600, L11
Bell, E.F. et al. 2004b, ApJ, 608, 752
Bell, E.F. et al. 2012, ApJ, 753, 167
Bendo, G. et al. 2015, MNRAS, 448, 135
Barden, M. et al. 2005, ApJ, 635, 959
Bournaud, F., Elmegreen, B.G. and Elmegreen, D.M. 2007, ApJ, 670, 237
Bourne, N. et al. 2015, in preparation
Bruce, V.A. et al. 2012, MNRAS, 427, 1666
Bruce, V.A. et al. 2014, MNRAS, 444, 1660
Buitrago, F., Trujillo, I. Conselice, C.J. & Haussler, B. 2013, MNRAS, 428, 1460
Burgarella, D. et al. 2013, A.&A., 554, 70
Cambresy, L., Reach, W.T., Beichman, C.A. & Jarrett, T.H. 2001, ApJ, 555, 563
Chen, H.-W. et al. 2003, ApJ, 586, 745
Combes, F. 2014, *Structure and Dynamics of Disk Galaxies*, eds M.S. Seigar and P. Treuthardt, ASP Conference Series, 480, 211
Cortese, L. 2012, A&A, 543, 132
Da Cunha, E., Charlot, S. & Elbaz, D. 2008, MNRAS, 388, 1595
Daddi, E. et al. 2005, ApJ, 626, 680
de Vaucouleurs, G. 1948, Ann d'Ap, 11, 247
Dekel, A. & Burkert, A. 2014, MNRAS, 438, 1870
Dole, H. et al. 2006, A&A, 451, 417
Driver, S.P., Popescu, C.C., Tuffs, R.J., Graham, A., Liske, J. & Baldry, I. 2008, ApJL, 678, L101
Driver, S.P. et al. 2011, MNRAS, 413, 971
Dwek, E. & Krennrich, F. 2013, Astroparticle Physics, 43, 112
Dye, S. et al. 2009, ApJ, 703, 285
Eales, S.A. et al. 2010, PASP, 891, 499
Eales, S.A. et al. 2015, MNRAS, in preparation
Emsellem, E. et al. 2011, MNRAS, 414, 888
Elbaz, D. et al. 2011, A&A, 533, 119
Faber, S.M. et al. 2007, ApJ, 665, 265
Fixsen, D.J. et al. 1998, ApJ, 508, 128
Genzel, R. et al. 2011, ApJ, 733, 30
Genzel, R. et al. 2014, ApJ, 785, 75
Graham, A.W. & Guzman, R. 2003, AJ, 125, 2936
Graham, A.W. and Driver, S.P. 2005, PASA, 22, 118
Graham, A.W. and Worley, C.C. 2008, MNRAS, 388, 1708
Graham, A.W. 2013, in *Planets, Stars and Stellar Systems*, Volume 6, p91-140, eds T.D. Oswalt and W.C. Keel, Springer Publishing (arXiv: 1108.0997)
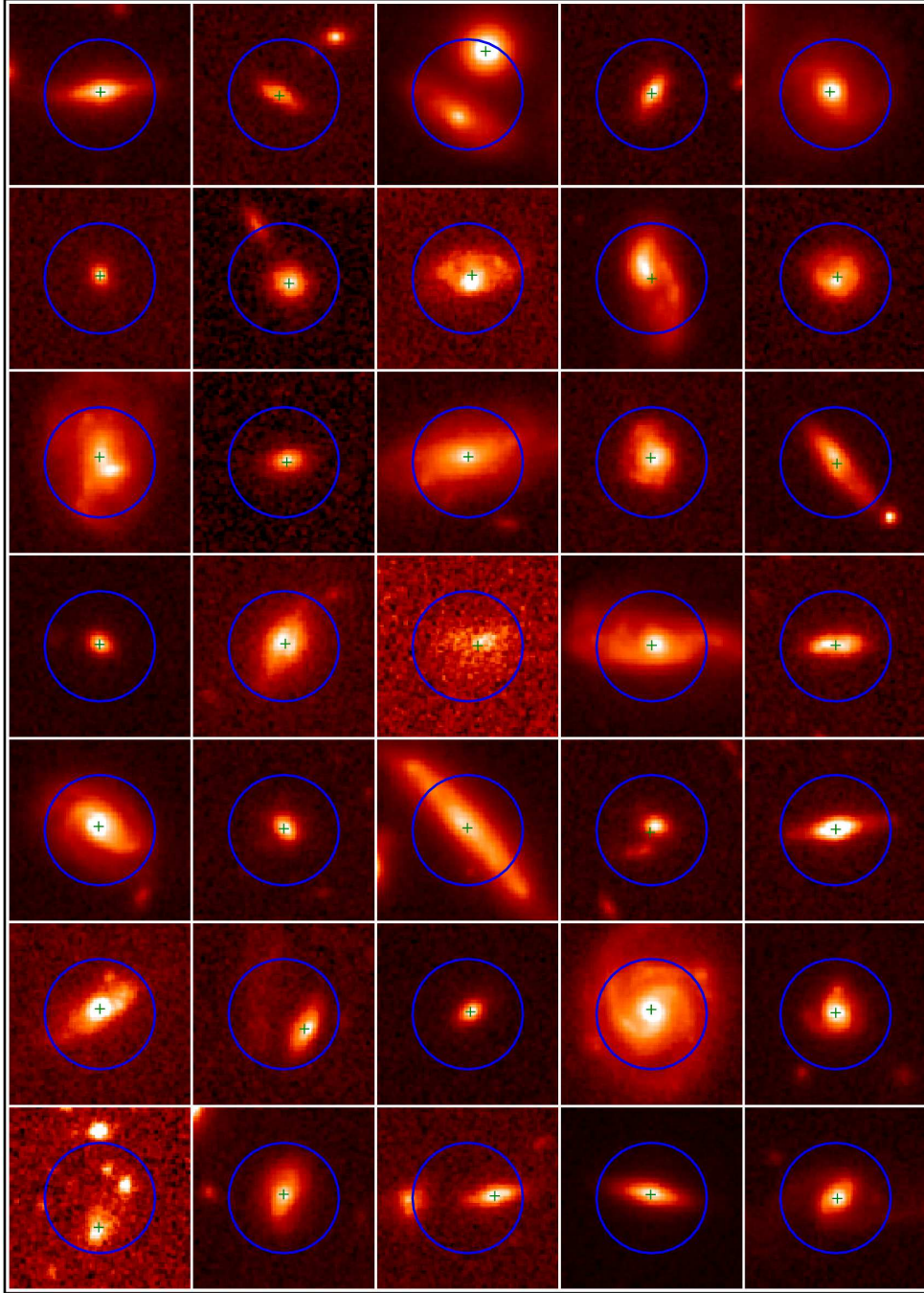
Graham, A.W., Dullo, B.T. & Savorgnan, G.A.D., MN-RAS, in press (arXiv: 1502.07024)

Guo, Y. et al. 2013, ApJ Suppl. 207, 24

Hopkins, A. & Beacom, J.F. 2006, ApJ, 651, 142

Hubble, E.P. 1926, ApJ, 64, 321

Hubble, E.P. 1927, The Observatory, 50, 276

Ibar, E. et al. 2010, MNRAS, 409, 38

Ilbert, O. et al. 2013, A.&A. 556, 55

Kelvin, L.S. et al. 2012, MNRAS, 421, 1007

Kelvin, L.S. et al. 2014a, MNRAS, 439, 1245

Kelvin, L.S. et al. 2014b, MNRAS, 444, 1647

Kennicutt, R.C. 1998, ARAA, 36, 189

Kennicutt, R.C. & Evans, N.J. 2012, ARAA, 50, 531

Koekemoer et al. 2011, ApJ Suppl. 197, 36

Krajnovic, D. et al. 2013, MNRAS, 432, 1768

Laurikainen, E., Salo, H., Buta, R., Knapen, J.H. & Comerón, S. 2010, MNRAS, 405, 1089

Lee, B. et al. 2013, ApJ, 774, 47.

Leitner, S.N. & Kravtsov, A.V. 2011, ApJ, 734, 48

Leiton, R. et al. 2015, A.&A. in press (arXiv: 1503.05779)

Levenson, L.R., Wright, E.L., Johnson, B.D. 2007, ApJ, 666, 34

Li-Ting, H. et al. 2014, arXiv: 1409.7119v1

Lilly, S.J. & Cowie, L.L. 1987, *Infrared astronomy with arrays, Proceedings of the Workshop on Ground-based Astronomical Observations with Infrared Array Detectors, held at University of Hawaii, Hilo, March 24-27, 1987,* edited by C.G. Wynn-Williams and E.E. Becklin, 473

Magnelli, B. et al. 2013, A&A, 553, 132

Martig, M., Bournaud, F., Teyssier, R. & Dekel, A. 2009, ApJ, 707, 250

Maraston, C. 2006, MNRAS, 362, 799

Marsden, G. et al. 2009, ApJ, 707, 1729

Martin, D. et al. 2005, ApJ, 619, L1

Muzzin, A. et al. 2013, ApJ, 777, 18

Nguyen, H.T. et al. 2010, A&A, 518, L5

Noguchi, M. 1999, ApJ, 514, 77

Oliver, S. et al. 2012, MNRAS, 424, 1635

Pagel, B. 1997, *Nucleosynthesis and Chemical Evolution of Galaxies* (Cambridge)

Pascale, E. et al. 2011, MNRAS, 415, 911

Pilbratt, G. et al. 2010, A&A, 518, L1

Peng, Y.-J. et al. 2010, ApJ, 721, 193

Planck Collaboration XVI 2014, A & A, 571, 16 A&A submitted, arXiv: 1303.5706

Ravindranath et al. 2006, ApJ, 652, 963

Rigby, E.E. et al. 2011, MNRAS, 415, 2336

Sérsic, J.L. 1963, Boletin de la Asociacion Argentina de Astronomia, 6, 41

Shen, S., Mo, H.J., White, S.D.M., Blanton, M.R., Kauffmann, G., Voges, R., Brinkmann, J. & Csabai, I. 2003, MNRAS, 343, 978

Szomoru, D., Franx, M., Bouwens, R.J., Van Dokkum, P.G., Labbé, I., Illingworth, G.D. & Trenti, M. 2011, ApJ, 735, L22

Smith, D.J.B. et al. 2011, MNRAS, 416, 857

Smith, M.W.L. et al. 2012, ApJ, 748, 123

Smith, D.J.B. et al. 2012b, MNRAS, 427, 703

Tasca, L.A.M. et al. 2014, A&A, 564, 12

Takeuchi, T.T., Buat, V. & Burgarella, D. 2005, A.&A., 440, L17

Taylor, E.N. et al. 2011, MNRAS, 418, 1587

Toomre, A. 1977, *Evolution of Galaxies and Stellar Populations, Proceedings of a Conference and Yale University,* edited by B.M. Tinsley and R.B. Larson (Yale University Observatory, New Haven, Conn.), 401

Trenti, M. & Stiavelli, M. 2008, ApJ, 651, 142

Trujillo, I. et al. 2006, ApJ, 650, 18

Valiante, E. et al. 2015, in preparation

Van den Berg, S. 1976, ApJ, 206, 883

Van der Wel, A. et al. 2012, ApJ Suppl. 203, 24.

Van der Wel, A. et al. 2014, ApJ, 792, L6

Windhorst, R.A. et al. 2011, ApJ, 193, 27

Wuyts, S. et al. 2011, ApJ, 742, 20
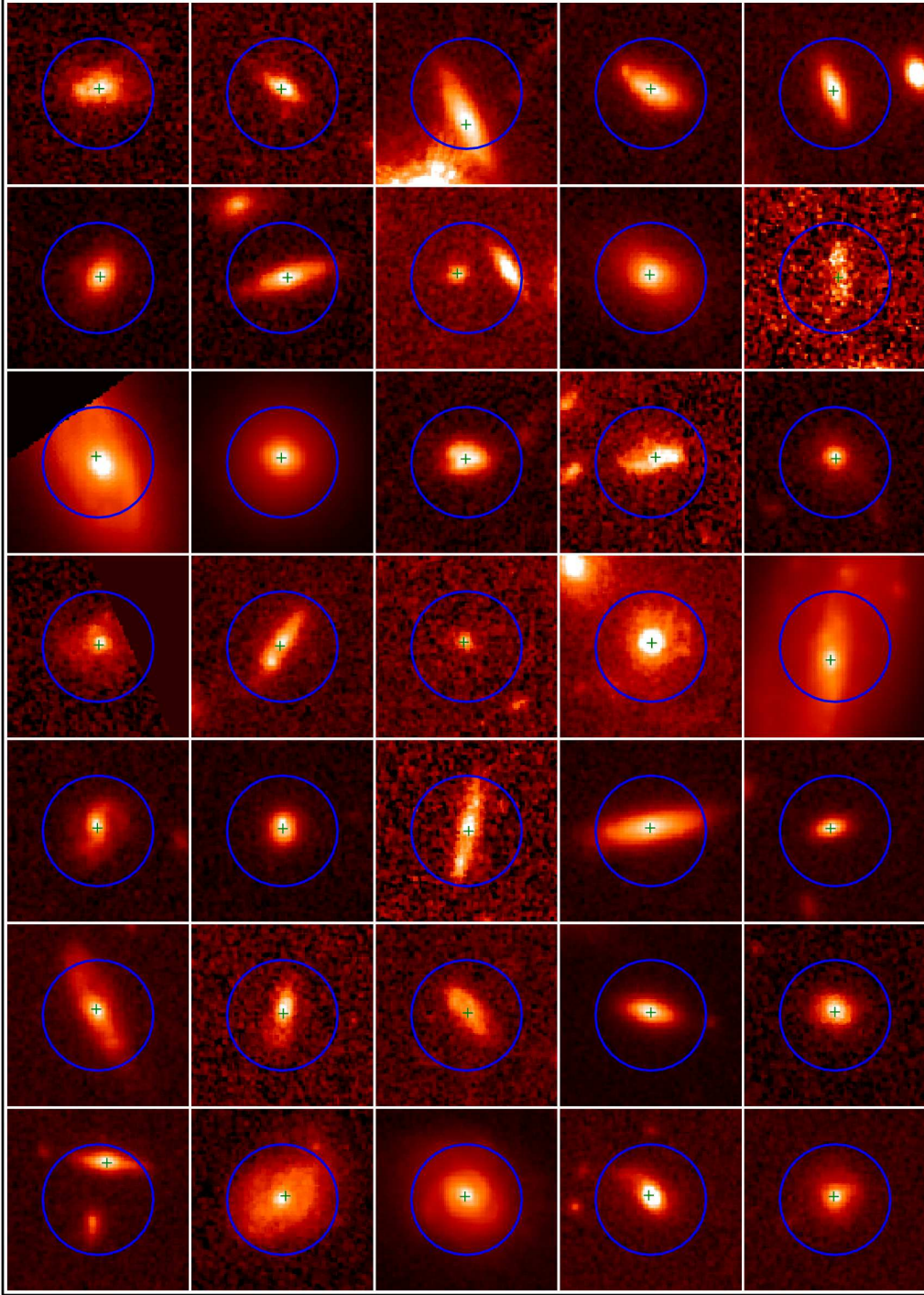
Figure 9. The H-band images (1.6 μm) of each of the Herschel sources in sample 1. The images are centred on the Herschel positions and have a size of 5×5 $arcsec^2$. The cross shows the near-infrared counterpart to the Herschel source that we have identified using our probabalistic analysis. The circle has a radius of 5 arcsec (the remaining sources are shown in the on-line version of the paper).
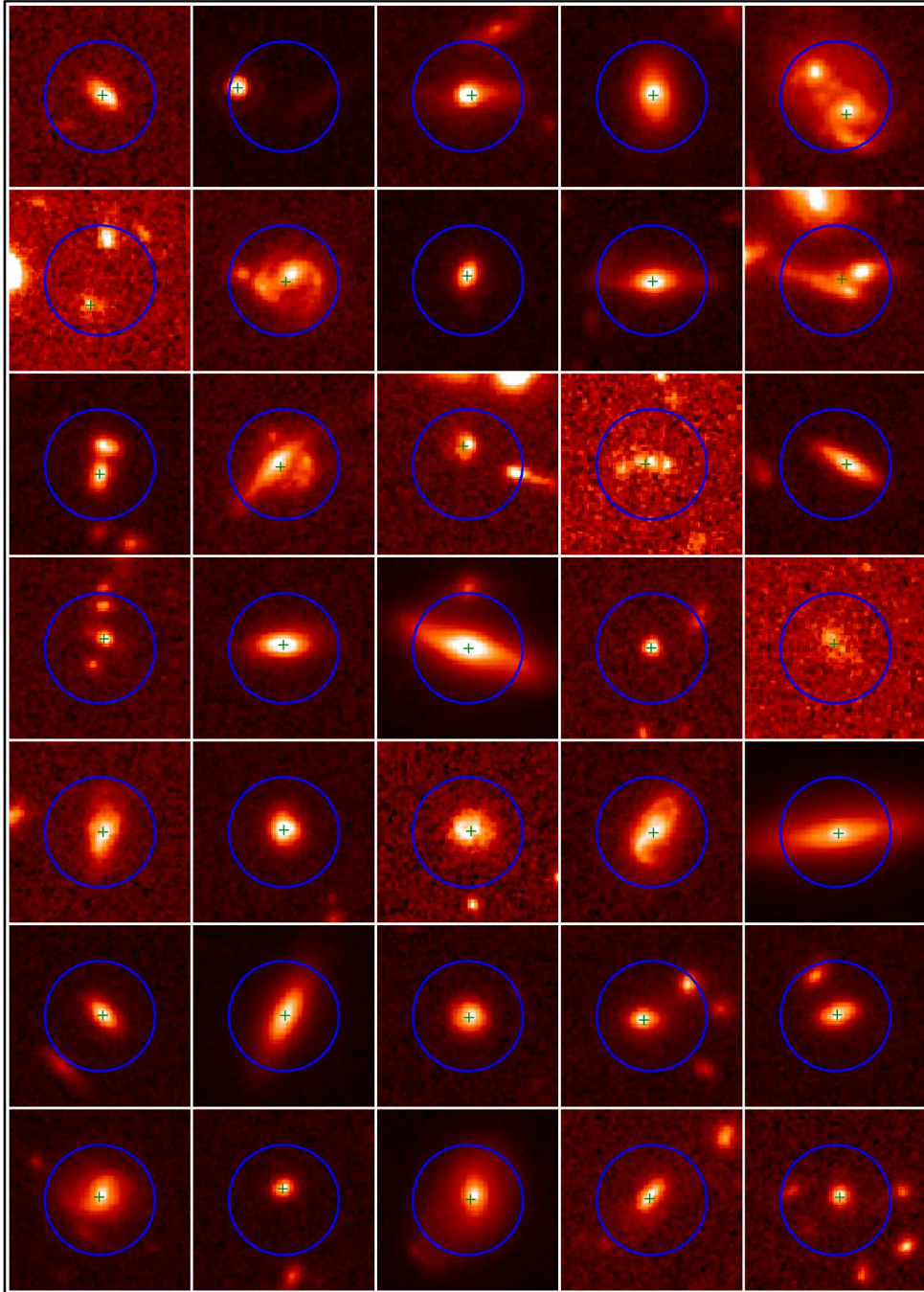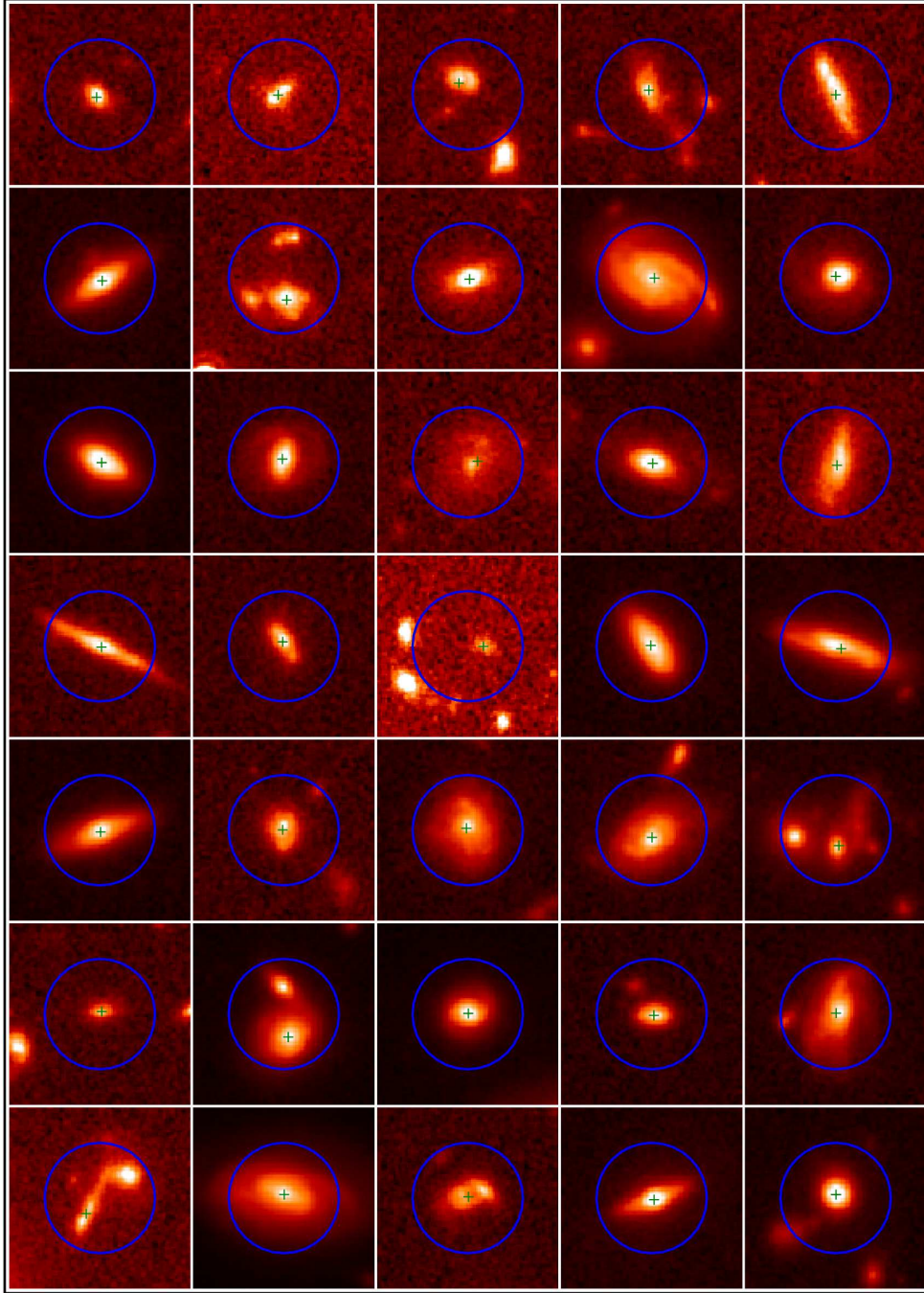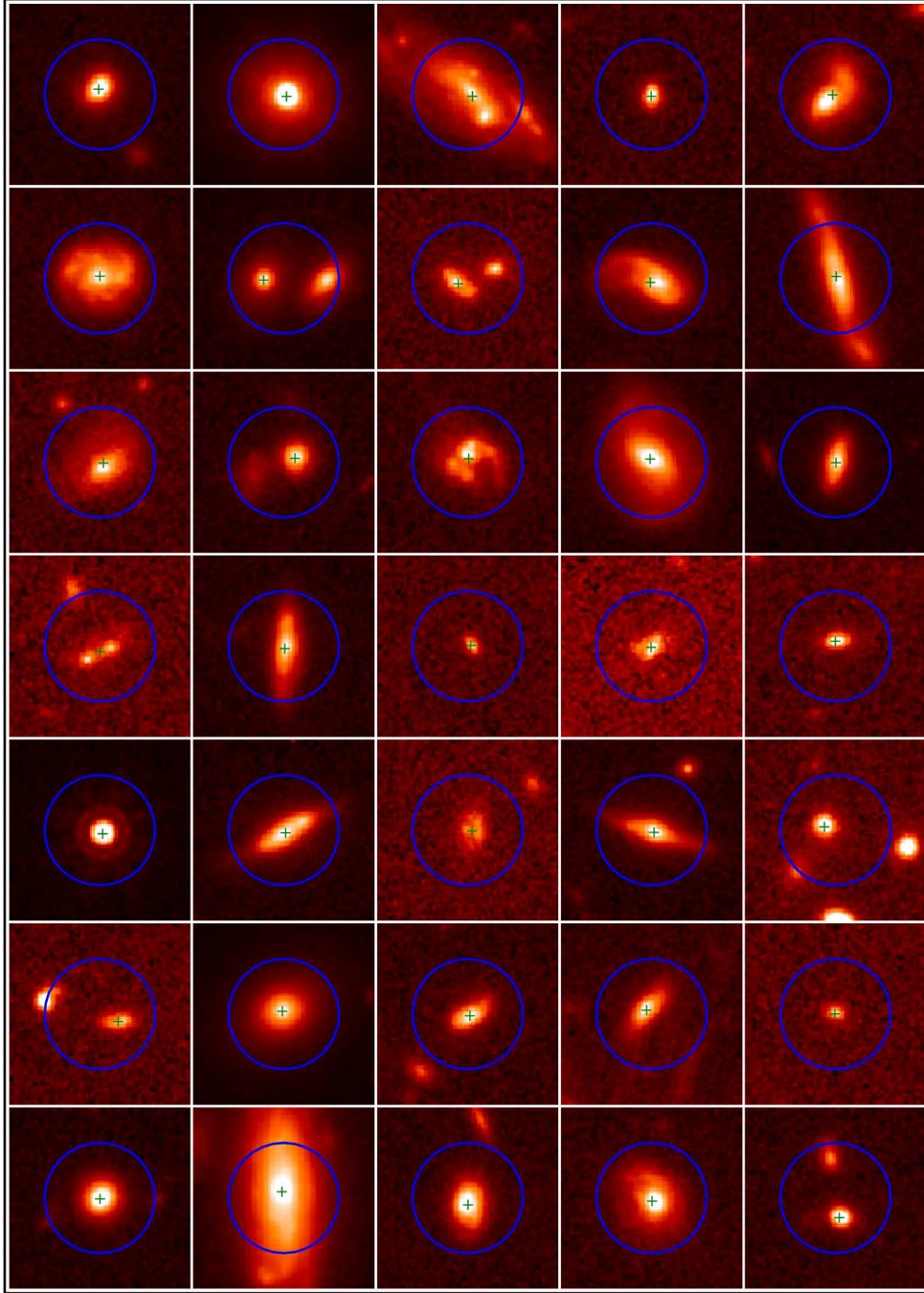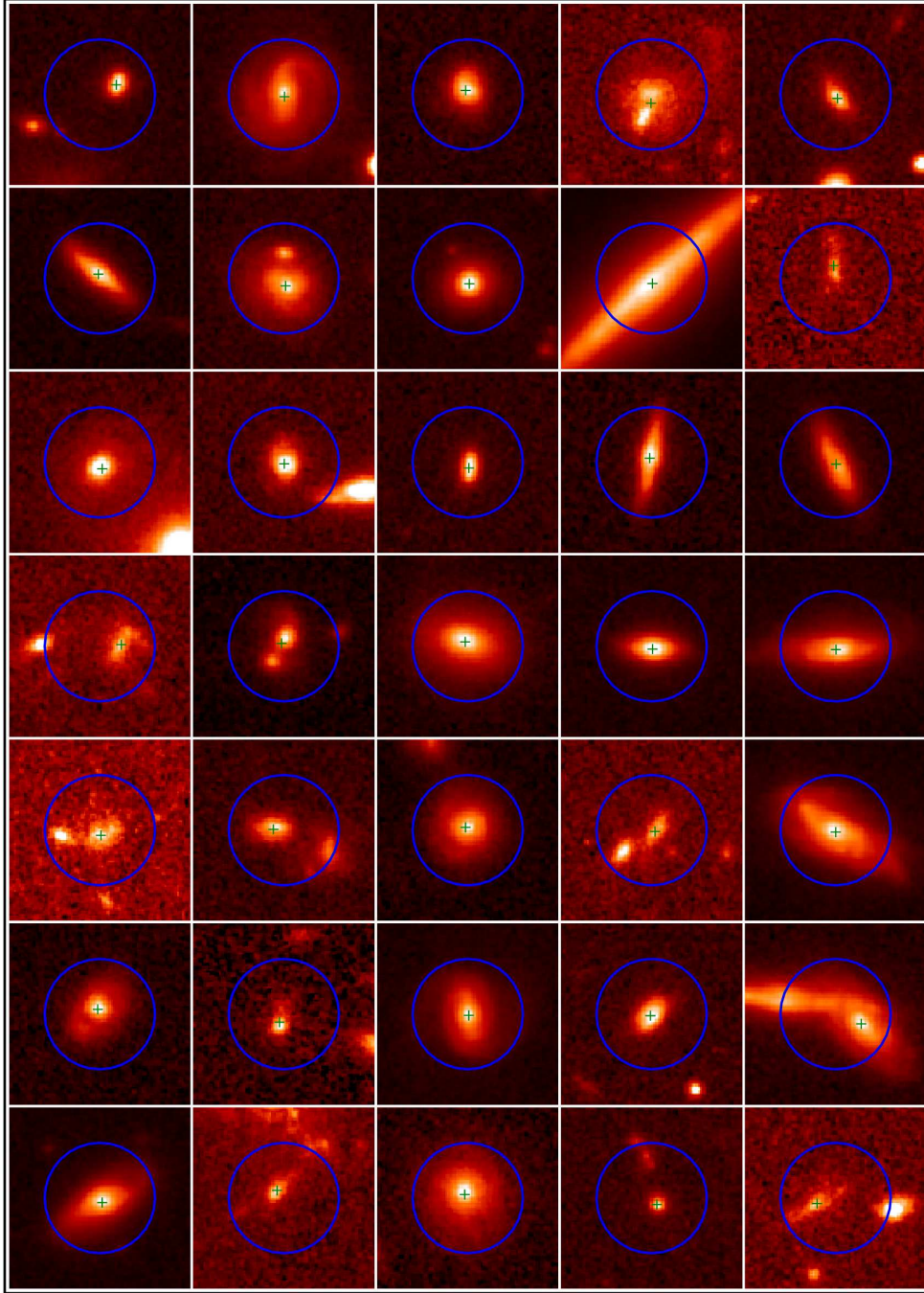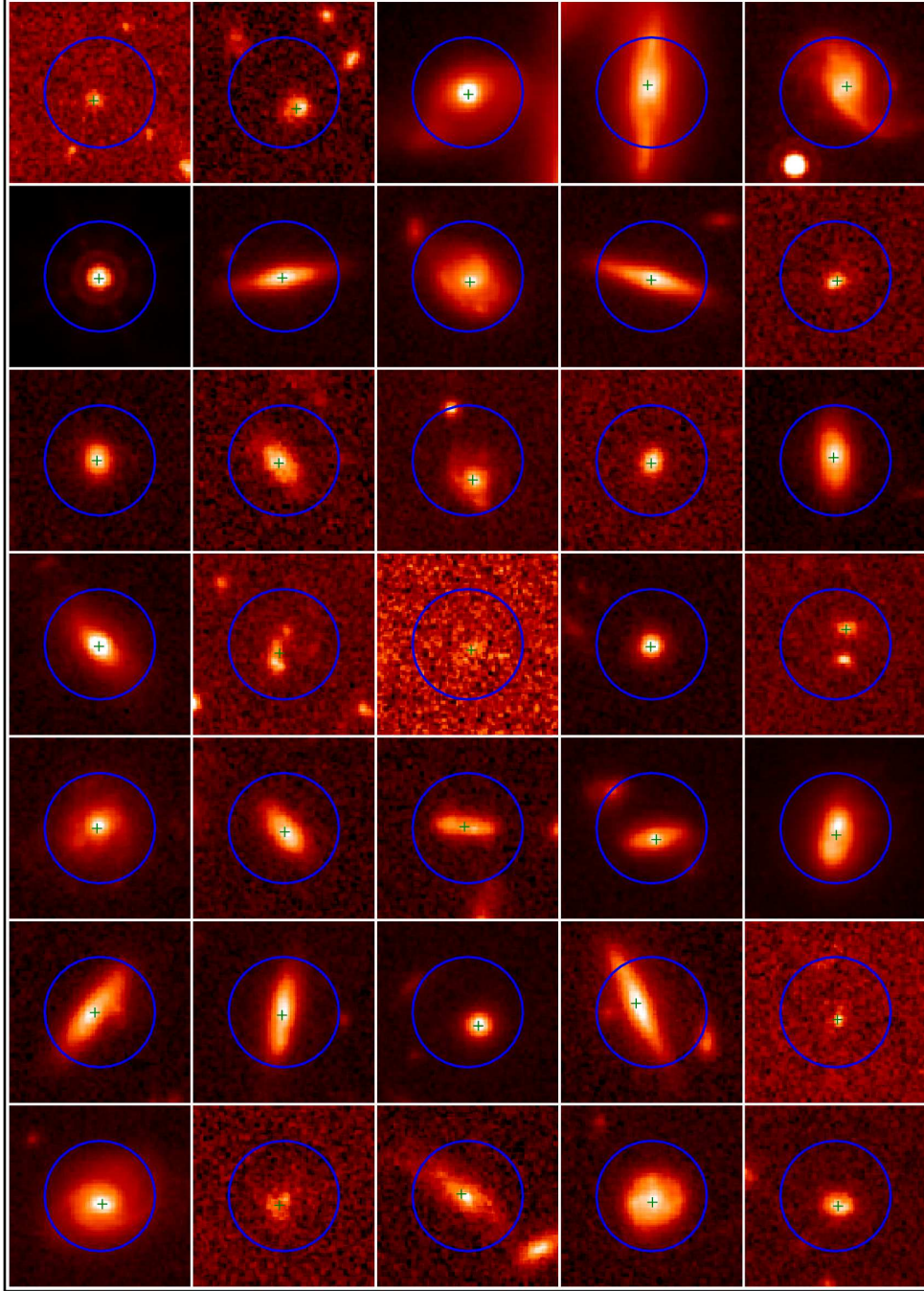
Figure 9 – *continued*

Figure 9 – *continued*
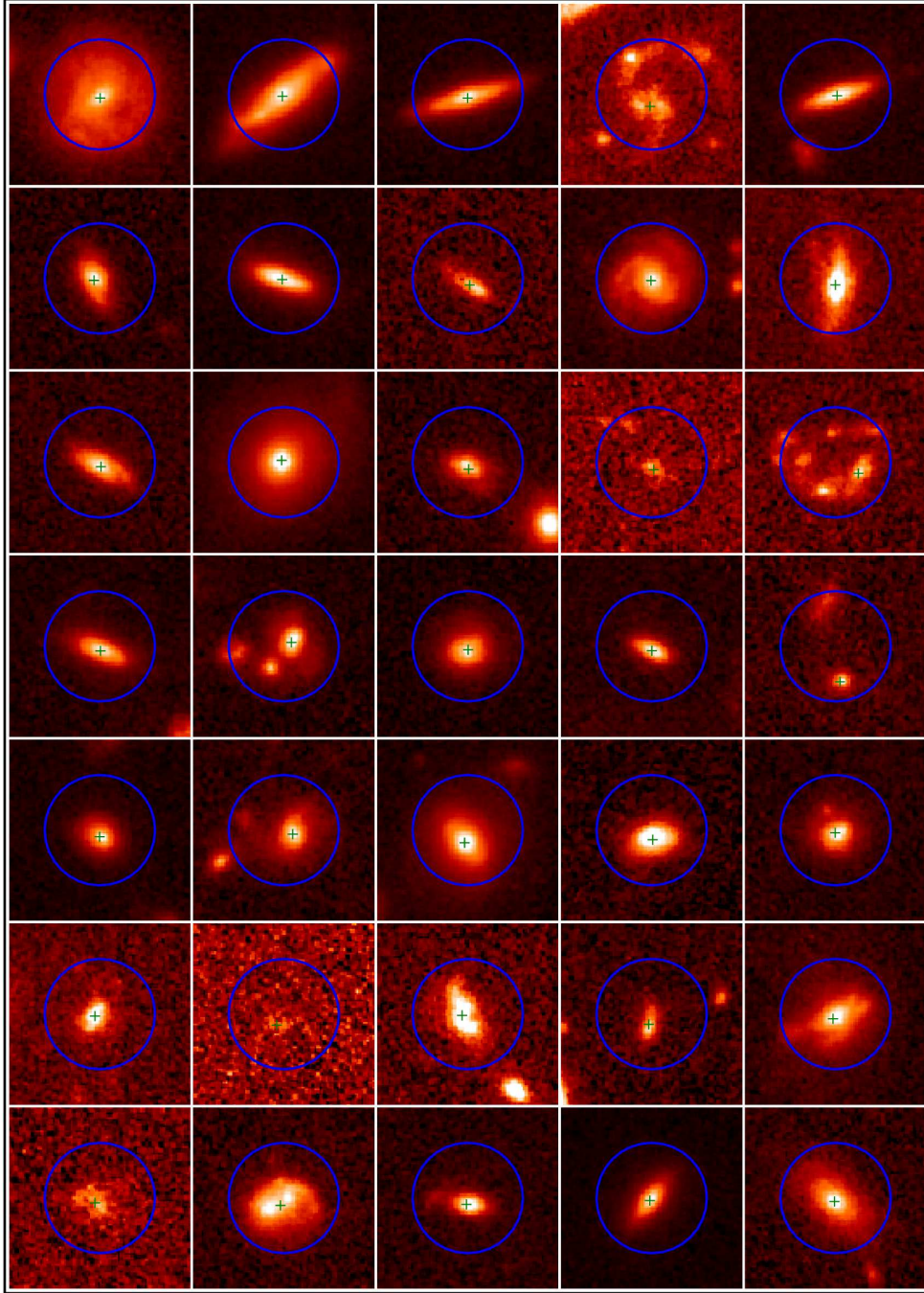
Figure 9 – *continued*

Figure 9 – *continued*

Figure 9 – *continued*

Figure 9 – *continued*

Figure 9 – *continued*

Figure 9 – *continued*

Figure 9 – *continued*

Figure 9 – *continued*

Figure 9 – *continued*